Brain state regulation during normal development: Intrinsic activity fluctuations in simultaneous EEG-fMRI

Lüchinger, Rafael ; Michels, Lars ; Martin, Ernst ; Brandeis, Daniel

Abstract: Brain maturation in adolescence is mirrored by the EEG as a pronounced decrease in low frequency activity. This EEG power attenuation parallels reductions of structural and metabolic markers of neuronal maturation (i.e., gray matter loss and decrease of absolute cerebral glucose utilization). However, it is largely unknown what causes these electrophysiological changes, and how this functional reorganization relates to other functional measures such as the fMRI BOLD signal. In this study, we used simultaneously recorded EEG and fMRI to localize hemodynamic correlates of fluctuating EEG oscillations and to study the development of this EEG-BOLD coupling. Furthermore, the maturational EEG power attenuation was directly compared to BOLD signal power maturation. Both analyses were novel in their developmental perspective and aimed at providing a functional lead to EEG maturation. Data from 19 children, 18 adolescents and 18 young adults were acquired in 10min eyes-open/eyes-closed resting states. Our results revealed that both EEG and BOLD amplitudes strongly decrease between childhood and adulthood, but their functional coupling remains largely unchanged. The global reduction of absolute amplitude of spontaneous slow BOLD signal fluctuation is a novel marker for brain maturation, and parallels the globally decreasing trajectories of EEG amplitudes, gray matter and glucose metabolism during adolescence. Further, the absence of thalamocortical EEG-BOLD coupling in children together with age-related normalized thalamic BOLD power increase indicated maturational changes in brain state regulation.

DOI: https://doi.org/10.1016/j.neuroimage.2012.01.031

Brain State Regulation During Normal Development: Intrinsic Activity Fluctuations In Simultaneous EEG–FMRI

Published as: *Lüchinger R, Michels L, Martin E, Brandeis D, (2012). Brain state regulation during normal development: Intrinsic activity fluctuations in simultaneous EEG-fMRI. Neuroimage, 60, 1426-1439.*

Abstract **- Brain maturation in adolescence is mirrored by the EEG as a pronounced decrease in low frequency activity. This EEG power attenuation parallels reductions of structural and metabolic markers of neuronal maturation (i.e., gray matter loss and decrease of absolute cerebral glucose utilization). However, it is largely unknown what causes these electrophysiological changes, and how this functional reorganization relates to other functional measures such as the fMRI BOLD signal. In this study, we used simultaneously recorded EEG and fMRI to localize hemodynamic correlates of fluctuating EEG oscillations and to study the development of this EEG–BOLD coupling. Furthermore, the maturational EEG power attenuation was directly compared to BOLD signal power maturation. Both analyses were novel in their developmental perspective and aimed at providing a functional lead to EEG maturation. Data from 19 children, 18 adolescents and 18 young adults were acquired in 10 min eyes-open/eyes-closed resting states. Our results revealed that both EEG and BOLD amplitudes strongly decrease between childhood and adulthood, but their functional coupling remains largely unchanged. The global reduction of absolute amplitude of spontaneous slow BOLD signal fluctuation is a novel marker for brain maturation, and parallels the globally decreasing trajectories of EEG amplitudes, gray matter and glucose metabolism during adolescence. Further, the absence of thalamocortical EEG–BOLD coupling in children together with age-related normalized thalamic BOLD power increase indicated maturational changes in brain state regulation.**

Introduction

Human brain maturation is mirrored by changes in the resting electroencephalogram (EEG). The EEG power decreases between late childhood and early adulthood as a curvilinear function of age, most prominently in low frequencies which have been documented

extensively for over 60 years (Boord et al., 2007; Dustman et al., 1999; Eeg-Olofsson, 1970; Gasser et al., 1988; Gibbs and Knott, 1949; Matousek and Petersen, 1973; Matsuura et al., 1985; Somsen et al., 1997) and have been related to cognitive maturation (Case, 1992; John et al., 1980; Thatcher, 1994; Wackermann and Matousek, 1998). The maturational power decrease is a global phenomenon (Whitford et al., 2007); typically affecting all scalp sites, although its effect in additional topographical features has been noted (Gasser et al., 1988).

Oscillatory activity in the EEG at rest (i.e. in the absence of task or stimulation) demonstrates that the brain is far from resting. The enormous intrinsic energy consumption exceeds by far the additional costs associated with momentary demands of the environment (which may be as little as 0.5 to 1.0 % of the total energy budget) (Raichle, 2006). EEG oscillations arise from synchronized mass activity of mainly cortical neuron populations. Resting state EEG oscillations are typically subdivided into different bands such as low frequencies delta (1 - 4 Hz) and theta (4 - 8 Hz) and higher frequencies alpha (8 - 12 Hz) and beta (13 - 30 Hz). In general, increased low frequency power is a typical phenomenon in lower arousal functional states such as sleep (Cajochen et al., 2002; Campbell and Feinberg, 2009), neuropathology (Llinas et al., 2005; Llinas et al., 1999) or sedation (John et al., 2001). During resting states, the oscillatory compound reflects changes in brain states as indicated by shifts in arousal and alertness (Klimesch, 1999).

It is largely unknown which neuronal process guides the partly low-frequency-specific decrease in the EEG. Despite evidence that synchronized postsynaptic mass activity of aligned cortical neurons is the main source of the EEG, and that inhibitory activity and different cell types may contribute to higher frequencies, the exact generation and functional mechanisms of EEG oscillations are not fully understood (Brandeis et al., 2009). EEG changes, therefore, have been related to other neuronal measures. Brain development roughly shows a linear increase in global white matter volumes and an inverted U-shaped developmental trajectory for global gray matter structures, with peak volumes occurring in late childhood or early adolescence (Giedd et al., 1999; Gogtay and Thompson, 2010). Gray matter loss is a global phenomenon with lower order cortices maturing prior to higher order cortices (Gogtay et al., 2004). State independent, general mechanisms are also implicated by the fact that global EEG power decrease parallels maturational trajectories in sleep (Buchmann et al., 2011) and awake resting state (Whitford et al., 2007). Gray matter decrease reflects synaptic pruning (Bourgeois and Rakic, 1993; Huttenlocher, 1979), which presumably eliminates redundant connections and may be disrupted in adolescent psychiatric diseases (Paus et al., 2008). Physiologically, synaptic density may affect EEG power, as synaptic density reflects the connectivity and size of neuron populations from which EEG power partly derives (Boord et al., 2007; Feinberg and Campbell, 2010). Synaptic density also affects glucose metabolism, as the major portion of glucose maintains resting potentials (Chugani, 1998). Hence, absolute metabolic rates were found to parallel gray matter maturation in terms of cortical glucose uptake (Chugani, 1998; Chugani et al., 1987) and cerebral hemodynamic perfusion (Biagi et al., 2007), even though some maturational changes remain evident

after controlling statistically for gray matter density (Taki et al., 2011). The common global maturational decrease in electrical activity, neuronal density and metabolic energy budget has been highlighted (Boord et al., 2007; Feinberg and Campbell, 2010; Feinberg et al., 1990) referring to a general neuroregressive phenomenon (Chugani, 1998; Cowan et al., 1984). Metabolism is more closely related to the EEG in that it reflects brain function rather than structure. A close functional relation has also been demonstrated between electrophysiology and fMRI (Logothetis et al., 2001). Although BOLD-fMRI (blood-oxygen-level-dependency functional magnetic resonance imaging) has come to dominate human functional neuroscience, there is no study assessing the maturation of the relationship between EEG amplitudes and BOLD signals (neither in terms of the covariation of the fluctuating signals nor in quantitative terms of absolute signal amplitudes).

The fMRI BOLD signal is a slow hemodynamic correlate of activation that increases where neuronal activity increases (Logothetis et al., 2001; Niessing et al., 2005; Nir et al., 2007). Conventional fMRI studies report both increases as well as decreases in local BOLD activity as maturational correlate of cognitive functions (Blakemore and Choudhury, 2006), depending on the specific task, brain region and developmental phase. A general developmental trend "from diffuse to focal" may better account for the findings (Blakemore and Choudhury, 2006; Brown et al., 2006; Dick et al., 2006; Durston et al., 2006). Still, the maturational interpretation of increasing or decreasing activity or spatially diverse activity patterns is limited by confounding factors such as cognitive effort, experience or strategy (Casey et al., 2005). More recent fMRI research has focused on resting state brain activity in terms of functional connectivity (Biswal et al., 1995; Friston, 2002) between brain regions. This research approach has revealed resting state networks (RSNs) which are based on the spontaneously yet coherently fluctuating BOLD signal, and which are interpreted on the functional connotation of the anatomical structures that constitute the RSNs (Damoiseaux et al., 2006). In terms of development, the RSNs in awake children were found to be established as early as the age of 7 - 9 years (Fair et al., 2009; Supekar et al., 2009). After this age, maturational changes were described as more subtle fine tuning of within- and between-network connectivity (Dosenbach et al., 2010; Fair et al., 2009; Fair et al., 2007; Jolles et al., 2011; Supekar et al., 2009).

Large-scale networks of coherently fluctuating BOLD signals, of which now up to ten have been consistently identified (Damoiseaux et al., 2006; Deco et al., 2011), were first observed during passive rest but their activity continues during cognitive engagement (e.g. task or stimulation) with a high topographical correspondence (Calhoun et al., 2008; Mennes et al., 2010; Smith et al., 2009; Thomason et al., 2008). On an arousal continuum, rest can be seen as an intermittent state between sleep and attention, which itself transiently fluctuates subtly along the arousal scale. Both EEG and fMRI reflect arousal-related features of resting brain state regulation. In the EEG, the sensitivity is reflected by the oscillatory composition (Olbrich et al., 2009; Sadaghiani et al., 2010). Resting state fMRI features two major (and antagonistic) RSNs, the default mode network (DMN) (Raichle et al., 2001; Raichle and Snyder, 2007) and the attention

network (ATN) (Fox et al., 2005) the activity of which reflects shifts along the arousal scale as their engagement relates to rest or attentional task activity. The physiological mechanism that regulates vigilance/arousal/alertness states is associated with thalamic activity and thalamocortical circuitry (Llinas et al., 1998; McCormick and Bal, 1997; Steriade et al., 1993). Evidence for human thalamocortical activity during rest has been obtained noninvasively by simultaneous recording of EEG and fMRI. These studies revealed that activity in the alpha range (10 Hz) is accompanied by BOLD activity in a thalamocortical network (TCN) with thalamus positively correlated and sensory areas negatively correlated (de Munck et al., 2007; Difrancesco et al., 2008; Feige et al., 2005; Goldman et al., 2002; Lüchinger et al., 2011; Moosmann et al., 2003; Tyvaert et al., 2008). Such functional coupling is typically based on temporal correlation of frequency-specific EEG power fluctuations (convolved with the slow hemodynamic response function) with the co-registered regional BOLD signal in eyes-closed resting state. Functional coupling of EEG oscillations in different frequencies was also found in regions comprising the DMN (Lüchinger et al., 2011; Scheeringa et al., 2008) and the ATN (Laufs et al., 2006; Laufs et al., 2003; Lüchinger et al., 2011). Both resting with eyes-open (EO) or eyes-closed (EC) refer to passive baseline activity (Gusnard and Raichle, 2001). EO condition increases arousal more than EC condition (Barry et al., 2009; Barry et al., 2007) inducing an arousal gradient that allows for differentiation between state-dependent and state-independent effects. As simultaneous recording of EEG and fMRI allows for localizing functional correlates of EEG oscillations, it adds to the understanding of resting state brain function and may even reveal a functional correlate of EEG maturation. Apart from our own recent study on late maturation, EEG–fMRI correlates have not been studied from a developmental perspective. We hypothesize that the EEG–BOLD signal couplings differ between children and adults as a result of the drastic power decrease in the EEG.

We further compare for the first time EEG maturation to BOLD signal maturation in terms of absolute amplitudes. This appears to be the most logical and direct approach in terms of equivalent measures. In contrast to EEG–BOLD signal correlations, which only consider normalized fluctuations of activity, spectral power provides an absolute measure of activity. The spectral range of the spontaneously fluctuating BOLD signal that is associated with neuronal activity is about 0.01 to 0.1 Hz (Biswal et al., 1995; Cordes et al., 2001), corresponding to the activity range of RSNs (Fox and Raichle, 2007). In resting state fMRI, the spectral power has recently attracted a great deal of interest (e.g. Baria et al., 2011; Biswal et al., 2010; Duff et al., 2008; Horovitz et al., 2008; Yang et al., 2007; Zuo et al., 2010). While the BOLD signal power is usually normalized to reduce inter-subject variability, here we used absolute power to detect possible decreases in activity relating to development. We also used absolute power for an equivalent contrast to EEG power (relative power was examined in a subsidiary analysis). To our knowledge, maturation of BOLD amplitude has not been investigated yet. Despite the lack of literature, we anticipate a power decrease from childhood to adulthood. We base this expectation on the aforementioned decreasing neurodevelopmental trend that is common to structural and functional measures which likely relate to the BOLD signal.

In this study we thus examined EEG power and fMRI BOLD signal fluctuations for their functional coupling (i.e., temporal correlation), and compared their absolute signal amplitudes (i.e., spectral power). Both approaches are novel in the developmental context and aimed to capture markers of normal healthy brain development. We investigated the major EEG frequency bands and both resting states (EO/EC), as they proved to be important factors in EEG–BOLD signal correlations (Lüchinger et al., 2011), and allows to distinguish between state-dependent and state-independent developmental mechanisms.

Methods

Patricipants

We used the same groups of adults and adolescents as described in our previous report (Lüchinger et al., 2011) and additionally recruited a group of children. The original sample sizes used for analysis were reduced due to technical issues during scanning (3 adults, 2 adolescents), excessive head motion ($>$ 3 mm, 1 adolescent) and unsuccessful artifact rejection (1 child), resulting in 18 adults (mean age 25.3 $\pm$ 3.8 years, 8 males), 18 adolescents (mean age 15.9 $\pm$ 1.1 years, 8 males) and 19 children (mean age 10.6 $\pm$ 1.3 years, 8 males). The age statistics deviate slightly from the earlier publication due to more precise age calculation (monthly vs. years). All participants were right-hand dominant (Oldfield, 1971), had normal or corrected-to-normal vision, met the MRI safety standards and were healthy with no history of neurological or psychiatric disease. They were not taking drugs or medication currently, and they were asked to refrain from caffeine and nicotine consumption during the day of scanning. All participants, as well as the children's parents, gave written, informed consent prior to the investigation. The study was approved by the local ethics committee and was conducted in accordance with the guidelines determined in the Helsinki Declaration.

Procedure and recordings

The procedure, devices and data recording followed our published protocol (Lüchinger, Michels et al. 2011), and consisted of 10 min resting state simultaneous EEG–fMRI recording with alternating EO/EC blocks of 2.5 min. In contrast to the previous report, only the 10 min first session was analyzed in this study because not all children completed the 2nd session following our extended measurement protocol (up to this session, protocols were identical among the groups).

EEG analysis

EEG preprocessing and analysis were done using BrainVision Analyzer 1.05 (BrainProducts, Gilching, Germany). Gradient artifacts were removed by average artifact subtraction (Allen et al., 2000; Allen et al., 1998), lowpass-filtered at 70 Hz cutoff and downsampled from 5 kHz to 500 Hz. The ballistocardiogram artifact was attenuated using a very

similar subtraction method with artifact windows aligned on QRS complexes detected in ECG traces (Allen et al., 2000; Allen et al., 1998), using maximal covariance method, templates based on 10 consecutive pulse intervals, and individually estimated time delay for subtraction based on global field power (GFP) distribution (CBC Parameters, Version 1.1).

EEG was digitally bandpass-filtered (0.5 - 70 Hz, 24 dB/oct and 50 Hz Notch) and further downsampled to 256 Hz. Using ICA decomposition (Delorme and Makeig, 2004) with selective back projection, eye blinks (Jung et al., 2000) and residual gradient and ballistocardiogram artefacts were eliminated. The residual MR-gradient artefacts components were identified by their spectral peaks and their non-physiological topography (sharp asymmetry along the sagittal midline; scanner and cabling dependent). Residual ballistocardiac artefacts components were also identified by their characteristic topography (Debener et al., 2008). The same criteria were used for all age groups. Children and adolescents did not differ regarding residual EEG artefacts as judged by the total number of ICA components rejected (25.6 $\pm$ 6.45 versus 27.7 $\pm$ 8.1 out of 62), but fewer ICA components were rejected in adults (17.9 $\pm$ 3.0, $p < 0.01$ for both comparisons). The residual slice artefact at 18 Hz was suppressed by a narrow band rejection filter $\pm$ 0.5 Hz (Sadaghiani et al., 2010). All channels were then transformed to the average reference (Lehmann and Skrandies, 1980) and segments with remaining artefacts were marked for later rejection.

EEG power fluctuation. First, the EEG data set of each participant was parsed into EO and EC conditions. The conditions' onsets were defined individually by the exact time of opening and closing the eyes, as indicated by ICA component activation trace. For each volume acquisition (duration of 1.815 s), the absolute spectral power was calculated on each channel by a Fast Fourier Transformation (FFT) (Hanning window: 10 %, zero padded, 0.5 Hz resolution). Global spectral power (GSP) (Jann et al., 2009; Michels et al., 2010) was calculated for each FFT-transformed epoch as the root mean square across all channels. Hence, GSP is a measure of the total oscillatory activity over the scalp. The mean spectral band value was calculated for six common frequency bands comprising of delta (1 - 3 Hz), theta (4 - 7.5 Hz), alpha1 (8 - 9.5 Hz), alpha2 (10 - 13 Hz), beta1 (14 - 19 Hz) and beta2 (20 - 30 Hz) and the scan-to-scan fluctuation was used for correlation analysis with fMRI data after linear interpolation of epochs priorly marked as artifacts.

EEG mean power. Based on these steps, EEG amplitude was calculated as the mean of each FFT transformed epoch while epochs beforehand marked as artifacts were omitted. Group mean GSP was calculated for each condition and frequency band separately. Two-sample t-tests were used to calculate group differences (considered significant at $p < 0.05$, one-tailed, uncorrected for multiple comparisons). In addition, electrode-wise calculations allowed mapping power to illustrate its scalp topography. Group mean power maps as well as t-maps for group differences were calculated. A t-value of > 3.144 corresponds to $p < 0.05$ for one-sided group differences (Bonferroni corrected for 60 multiple tests within a map).

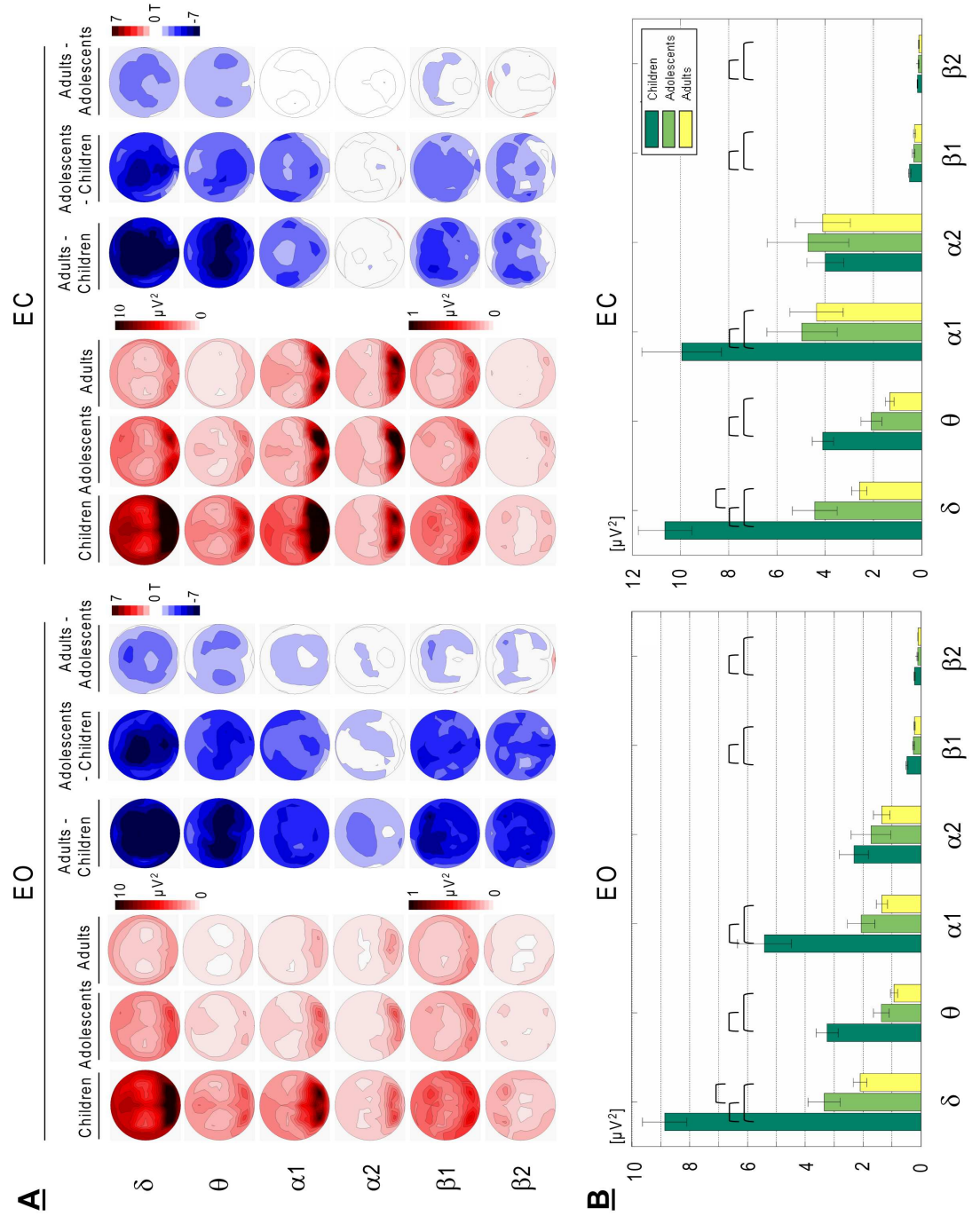

Fig. 2.1 EEG band power results. A: EEG topography and topographical group differences of EO and EC resting states. Group means are shown with color scaling. The spectrum follows a power law (compare B) necessitating a different scaling for beta1 and beta2. Contour lines indicate a step of 0.5 μV^2 and are based on triangulation and linear interpolations of the sixty scalp electrodes. Group differences are shown as t-maps with red (positive) to blue (negative) scaling. All t-maps range from 7 to -7 whereas all differences are calculated as 'younger group - older group'. Contour lines represent a step of ±1 t-value. A t-value of >= 3.144 corresponds to $p < 0.05$ for one-sided group difference, Bonferroni corrected for 60 multiple tests within a map. The top of the maps is anterior. B: The global spectral power (GSP) separated by group, condition and frequency. The bars represent mean power values in μV^2 and error bars reflect the standard error mean. The brackets indicate significant group differences (two-sample t-test, $p < 0.05$, one-tailed, uncorrected for multiple comparisons).

EEG–BOLD signal correlation

FMRI data preprocessing and analysis were done using SPM8 (Wellcome Department of Cognitive Neurology, London, UK). The images were realigned to the first scan by affine transformation and normalized into MNI standard space. They were resampled to 3 mm cubic voxels and spatially smoothed with 8 mm FWHM Gaussian kernel. The six head motion parameters together with mean white matter and cerebrospinal fluid signals were later used as nuisance covariates. Located by thresholded SPM8 template (> 70 %), cerebrospinal fluid was extracted from 5 mm spheres within ventricles [0, 11, 9; 0, -40, -2] (xyz MNI-coordinates) and white matter from anterior and posterior corpus callosum [0, -38, 13; 0, 26, 2].

EEG–BOLD signal correlations were calculated voxel-wise, using the SPM8 general linear model (GLM) approach. Each of the depicted frequency bands was analyzed in a separate model. The model consisted of two boxcar functions modeling EO and EC conditions which were parametrically modulated by the aforementioned GSP fluctuations. The opening and closing of the eyes introduce transition-specific motor and visual activity. This was seen here as confounding both EEG and fMRI resting-state signals, and was modeled in two additional regressors in an event-related manner. The standard hemodynamic response function was used to convolve the model regressors. A first-order autoregressive model accounted for serial correlations and a 128 s highpass filter eliminated very slow drifts. The model always contained the nuisance variables. The model was run for each participant, and the contrast image of the GSP regressor was written for subsequent group statistics.

A 3 x 2 x 6 full factorial design (Analysis of Variance, ANOVA) was used for random effects analysis, with factor group (adults, adolescents, and children), factor condition (EO, EC) and factor frequency (delta, theta, alpha1, alpha2, beta1, beta2). Post-hoc t-tests were calculated separately for groups, conditions and frequencies in both positive and negative directions. Group differences were calculated as simple contrasts between all three groups in both directions (younger $>$ $<$ older). All group differences were inclusively masked by the corresponding group mean correlation patterns of the groups involved in the contrast. This allowed constraining group differences only in regions with significant correlations in any of the two group means involved in a group contrast. However, all group differences were also calculated without masking. The group differences are sensitive to different kinds of maturation effects such as linear or non-linear trajectories (including (inverted) U-shaped trajectories peaking in adolescence). A 2 x 6 full factorial design with factor condition and frequency and the participant's age (monthly) as covariate was calculated to estimate more general, maturation independent EEG–BOLD signal correlation patterns.

In a second analysis (Lüchinger et al., 2011), all six GSP frequency bands were included simultaneously in one common GLM at the subject level. Such a model provides partial correlations and was also used to alternatively test the frequency specificity in the EEG–BOLD signal correlations. The partial correlation patterns resulting from the common GLM were analyzed identically to the main analysis on the group level with a group x condition x frequency ANOVA as well as a condition x frequency ANCOVA with age as

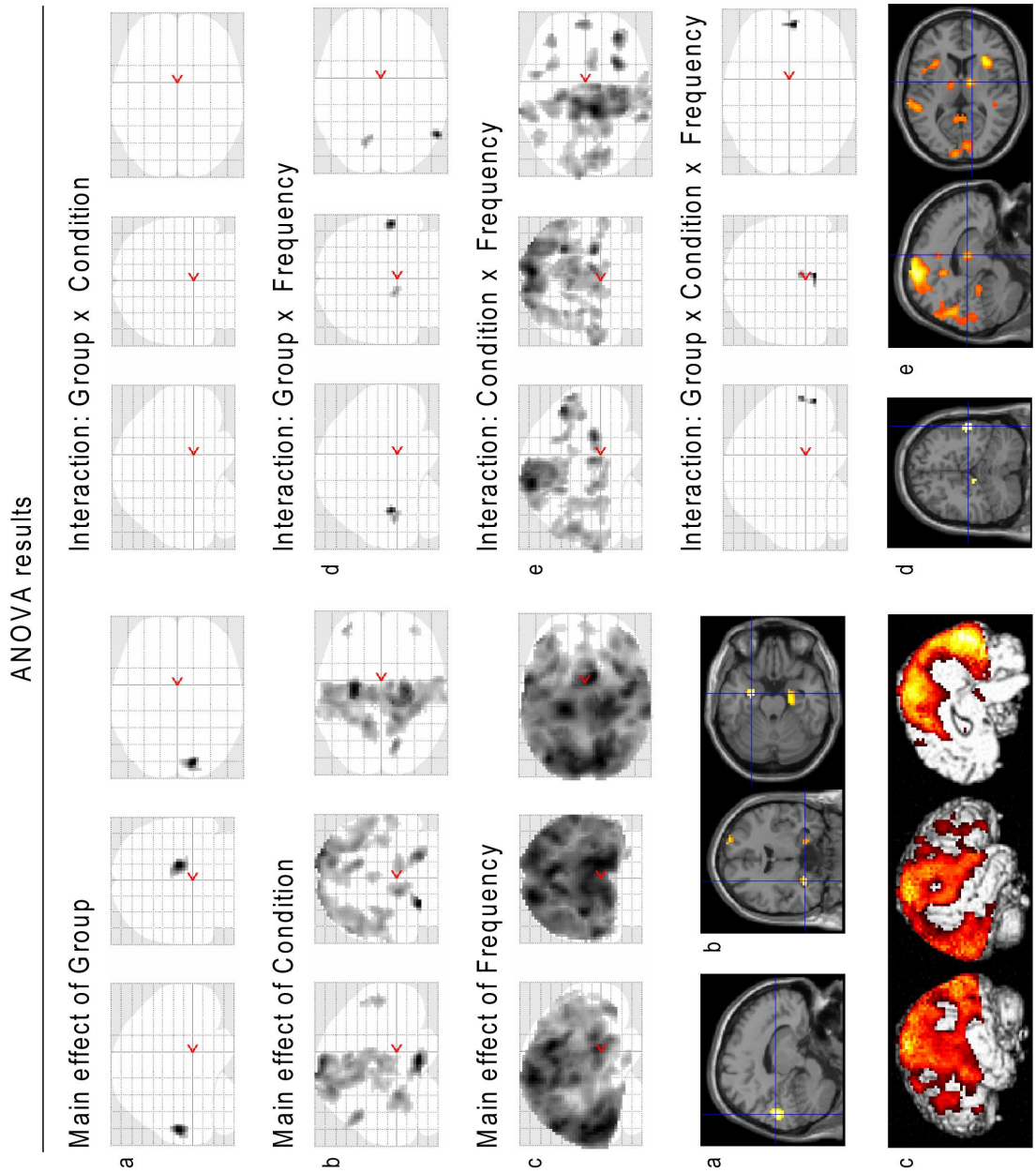

Fig. 2.2 ANOVA main effects and interactions of the EEG-BOLD correlation images resulting from the 3 groups by 2 conditions by 6 frequencies full factorial model. F-values are shown as maximum intensity projection in 'glassbrains' (saggital, coronal and axial views). Statistical height threshold was set to $p < 0.001$, corrected by extent threshold $k = 25$ voxels. To highlight topographical specificity, selected results were overplayed on SPM anatomical templates and labeled accordingly (a - e). Main effects of condition (b) and frequency (c) were thresholded at $p < 0.05$, FWE corrected, $k = 25$.

covariate. Results were considered significant at height threshold $p < 0.001$, corrected for multiple comparison by extent threshold of minimal cluster size of $k = 25$ voxels (Forman et al., 1995). The voxel extent threshold was calculated with Monte Carlo simulation (Slotnick et al., 2003).

BOLD signal spectral power analysis

BOLD signal spectral power was calculated on the same preprocessed images as used for EEG–BOLD signal correlation using REST toolbox V1.3 (http://restfmri.net). Prior to analysis, the six motion parameters were residualized from the images. REST calculates spectral power as ALFF (amplitude of low frequency fluctuation) (Yang et al., 2007; Zang et al., 2007). ALFF is the band average of the square-rooted FFT (taper percent = 0, FFT length = shortest). After removal of the linear trend, ALFF was calculated for the frequency range of 0.01 - 0.08 Hz for each participant separately for each condition. The BOLD spectral power is usually normalized spatially or even spectrally to reduce inter-subject variance. In order to coherently compare the maturing (absolute) EEG amplitudes to absolute amplitudes in the BOLD signal, the raw, non-normalized ALFF was used. However, the spatially normalized ALFF (mALFF = ALFF – mean(ALFF)) is more sensitive to regional differences, and was therefore calculated as well.

Group mean BOLD signal power was calculated for EO and EC conditions separately. Group differences were calculated condition-wise as two sample t-tests in both directions (younger <> older). The statistical threshold was set identically to the EEG–BOLD signal correlation analysis.

Results

EEG results

All groups' mean power maps revealed the typical resting state feature of pronounced posterior alpha power during EC (Fig. 2.1A) peaking around 10 Hz (Fig. 2.1B). Delta, theta and alpha1 showed a local power increase over middle frontal regions. The band-specific EEG topography appeared similar across groups. The t-maps confirmed the extensive, rather global topography of the power reduction with age, but also indicated a centrally maximal reduction for theta- and a fronto-centrally maximal reduction for delta and beta. This power reduction was most apparent in low frequencies and between children and adults, but extended to higher (beta) bands and was evident among adolescents and adults as well. GSP is a single global measure of frequency-specific EEG activity and was calculated to measure EEG–BOLD signal correlation. GSP profiles yielded the typical resting state's spectral profile (Fig. 2.1B). The t-tests confirmed significant GSP reduction between children and the two older groups for all frequency bands except for alpha2. The GSP reduction was significant between adolescents and adults in the delta band and approached significance in the theta band. Hence, GSP closely mirrored the maturational power decrease and together with the rather global topography of the EEG power decrease, GSP is an appropriate measure of EEG brain

maturation.

EEG–BOLD signal correlation results

The ANOVA main effects revealed that the EEG–BOLD signal correlations differed significantly among groups, conditions and frequencies (Fig. 2.2). Groups differed in one cluster in the occipital cortex. Conditions mainly differed along pre- and postcentral gyri and bilaterally in the hippocampus. Frequency effects were strongest in the occipital cortex, extending along dorsal and ventral streams, in pre- and postcentral gyri and in the lateral frontal cortex. Interactions were most apparent between condition and frequency. These results, which were also marked by distinct hemisphere symmetry, are listed in Supplementary Table S1.

EEG–BOLD signal correlations were subsequently calculated for each factor level separately (Fig. 2.3A). Overall, negative correlations dominated over positive correlations. Between groups, the correlations were robust as they reached significance in similar regions and in the same direction (correlation sign). Despite the weak ANOVA main effect on the groups, some critical patterns differed particularly between children and the older groups (adolescents and adults). In particular, children did not show a positive thalamic correlation in EC higher frequencies (alpha2, beta1, and beta2), not even at a very low statistical threshold. Across frequencies, differing correlation patterns appeared, consistent with the prominent frequency's main effect. Nevertheless, pattern redundancies between neighboring frequency bands emerged in some cases. The common model analysis clarified these redundancies (see below). Distinct differences appeared among lower and higher frequencies. In contrast to higher frequencies, the lower bands contained many more positive correlations. EO and EC conditions yielded different correlation patterns. Some portions appeared complementary between the conditions, such as the pre- and postcentral gyri. This is consistent with the ANOVA main effect of condition yielding the same structures.

Maturation-independent EEG–BOLD signal correlations were obtained by omitting the factor group and instead using age as covariate (Fig. 2.4 and Supplementary Table S3). EO delta power was positively correlated in the anterior cingulate cortex (ACC) and the anterior insula. Very similar correlations were found for EC delta but also for EO and EC theta. The theta band additionally showed widespread positive correlations along pre- and postcentral gyri and the adjacent superior frontal and superior temporal cortices. Visual inspection at lower statistical thresholds suggested that both low frequencies in both conditions share positive correlation to the cinguloopercular network (Dosenbach et al., 2007; Dosenbach et al., 2006). Negative correlations appeared for EO theta in the medial prefrontal cortex (MPFC), posterior cingulate cortex (PCC)/precuneus and bilaterally in inferior/superior lateral parietal cortex, together constituting the DMN, among other regions. Fractions of the DMN also exhibited negative correlations with EC theta and EO/EC delta, but these correlations were much less distinct and also involved other regions such as the middle/superior/inferior frontal gyrus. During EO, all higher frequencies from alpha1 to beta2 were negatively correlated in similar regions comprising portions of the occipital, parietal and frontal cortex and the posterior cingulate. This

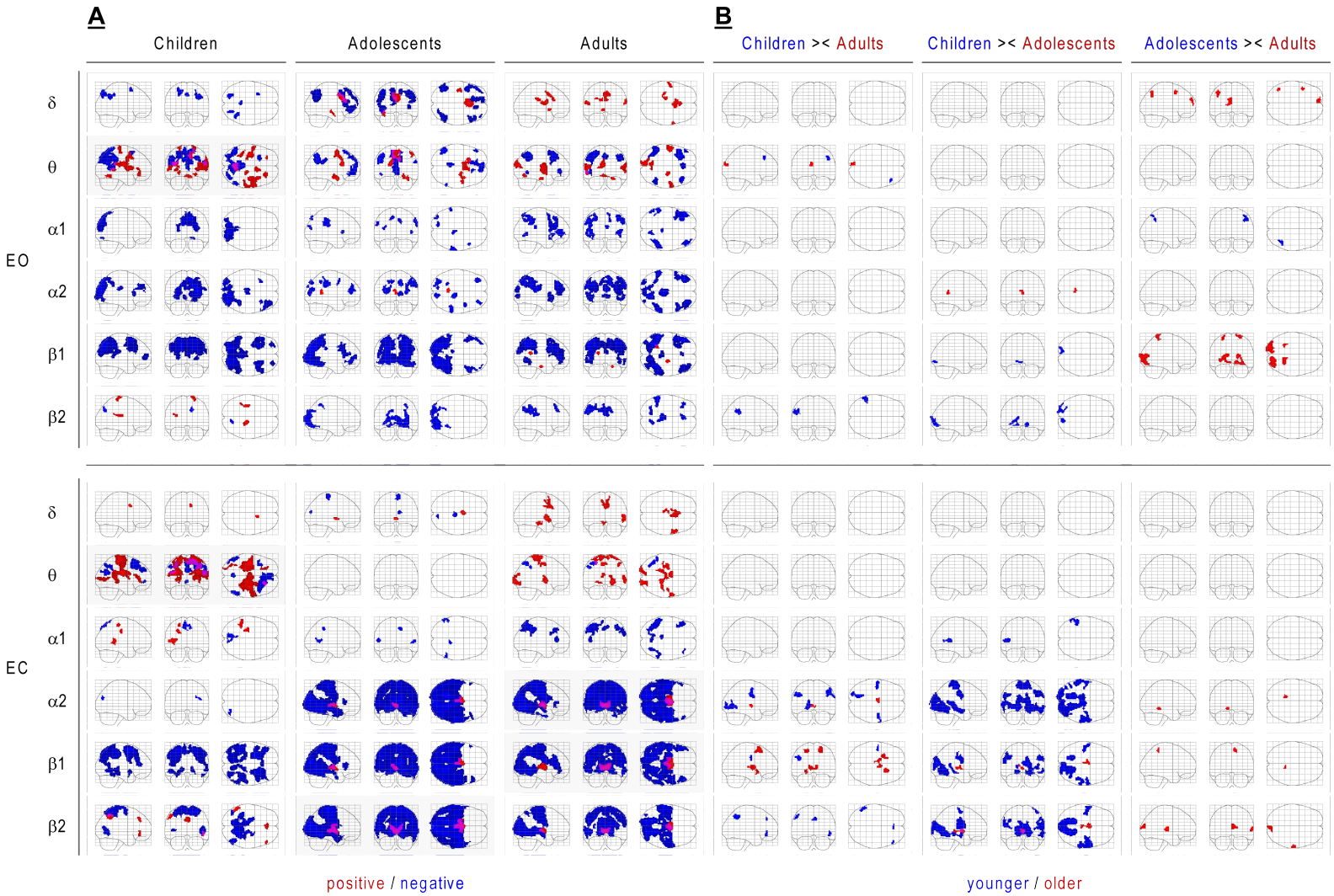

Fig. 2.3 Maturation of EEG-BOLD signal correlations. A: Group means by condition and frequency. T-values are shown as maximum intensity projection in 'glassbrains'. Positive correlations are scaled in red and negative correlations are scaled in blue. An overlay of red and blue colored voxels results in pink in the respective angle. B: Group differences of EEG-BOLD signal correlations separated by condition and frequency. Group differences are shown in both directions 'younger <> older' and color-coded as indicated by the column titles. All group differences were inclusively masked by the corresponding group mean correlation patterns of the groups involved in the contrast. A and B: Statistical height threshold was set to $p < 0.001$, corrected by extent threshold $k = 25$ voxels.

pattern was strongest for EO beta1 and overlaps with the ATN, especially in parietal and frontal areas. The only positive correlations appeared in the hippocampus with alpha1. During EC, the most salient correlation pattern appeared in the higher frequencies alpha2, beta1 and beta2. The pattern involved the positively correlated thalamus together with strong, widespread negative correlations in occipital, temporal, parietal, and frontal lobes. Although widespread, these negative correlations were limited to cortical regions, and excluded, for instance, the cingulate cortex, partly inferior parietal cortex, much of the frontal lobe and most of the sub-lobar regions.

The group differences of the correlation patterns are shown in Fig. 2.3B and listed in Supplementary Table S2. The most salient group difference was found in EC higher frequency bands alpha2, beta1 and beta2. Children had less negative correlations in cortical regions and less positive correlations in the thalamus (compared to adults in alpha2 and beta1, compared to adolescents in beta1 and beta2). Adolescents apparently had the strongest negative correlations. Despite this finding, only a few small, isolated or discontinuous group differences appeared. In order not to miss eventual weak yet more consistent maturation effects, the results were also inspected at a low statistical threshold ($p < 0.01$, $k = 0$, not shown).

The partial correlation patterns yielded similar overall results. The ANOVA (not shown) yielded a few more clusters for the main effect of group than the main analysis. The main effects of condition and frequency, and the condition x frequency interaction were similar in topography to those observed in the main analysis. Age-independent partial correlations are displayed in Fig. 2.4C. The negative DMN correlation appeared to be more specific for theta than for delta. The negative ATN correlation proved more specific for EO beta1 than for the neighboring bands. The low frequencies remained similar among conditions. The EC thalamocortical pattern was confirmed to be specific to all three higher frequency bands. The common model analysis produced more positive correlations across the group's mean patterns than the main analysis and overall reached slightly less statistical power. The group differences (not shown) were even fewer and the thalamocortical pattern no longer differed significantly. The children's negative EC theta-DMN correlation was stronger than in adolescents, but did not differ when compared to adults. Similar to the main analysis, the sparse group differences thus appeared isolated and did not reveal a continuous maturational trend for the correlations that would parallel power decrease in maturational low frequency EEG.

BOLD power results

Absolute BOLD signal power was much higher in gray matter than in white matter or cerebrospinal fluid. The power intensity projection mirrored the brain's gray matter structure (Fig. 2.5A). Topographically, the power distributions were similar across groups and conditions, but children showed higher power values. This group difference was highly significant in the direct group contrasts (Fig. 2.5B). In all comparisons, the younger group always exhibited more BOLD signal power than the older group. The other direction (older > younger) yielded no significant differences. Between children and the older groups, the power differences affected almost all brain regions. Between adolescents

and adults, the more subtle differences yielded a distinct topography with regions in the medial prefrontal cortex, posterior cingulate/precuneus and inferior parietal cortex. Compared to EO, these differences were slightly less pronounced.

The normalized power values revealed a very similar topography corresponding to gray matter anatomy. The group differences were much subtler and demonstrated high spatial specificity (Fig. 2.5C). Children were characterized consistently by significantly lower normalized BOLD power in the thalamus compared to both older groups in both conditions. Similarly, children showed significantly lower normalized power in the medial prefrontal cortex, posterior cingulate and left inferior parietal cortex compared to both older groups, especially during EO.

Discussion

General findings

The current study extends our earlier findings on late maturation to a younger age range including childhood (Lüchinger et al., 2011), and introduces a more comprehensive methodology including BOLD power analysis (matching the EEG analyses) to developmental fMRI work. Additional aspects of EEG–BOLD coupling maturation established here include generally consistent patterns across age groups but also frequency specific maturational differences.

Specifically, in comparison to (Lüchinger et al., 2011) the current study reveals three new findings. First, the functional coupling of cortical regions between spontaneous EEG power fluctuations and the BOLD signal is not only similar between adults and adolescents but also between school-aged children and older individuals in most frequency bands. Second, the absence of thalamocortical EEG–BOLD coupling in children, together with age-related normalized thalamic BOLD power increase, indicates that the EEG–BOLD coupling is not insensitive to maturation effects per se. Third, the absolute amplitude of spontaneous slow BOLD signal fluctuation reflects a marker for brain maturation, parallel to the globally decreasing trajectories of EEG amplitudes, gray matter and glucose metabolism during adolescence.

Brain development and EEG maturation

The low frequency EEG attenuation has a long tradition as a robust marker for functional brain maturation. Our data, recorded inside the MR scanner, strikingly confirm these findings. Strongest in lower frequencies with t-values up to 10 and higher, the power reduction was similar between EO and EC oscillations. Consistent with other studies (Boord et al., 2007; Kurth et al., 2010), this effect to a lower degree extended also to higher frequencies. According to previous publications, we do not believe that the observed EEG effects are massively influenced by changes of physical properties of the head (e.g., skull conductance or impedance) which change during early development, as these changes appear to be less prominent for the present age range (Hoekema et al., 2003). The fact that our developmental EEG amplitude reductions were frequency specific, and matched

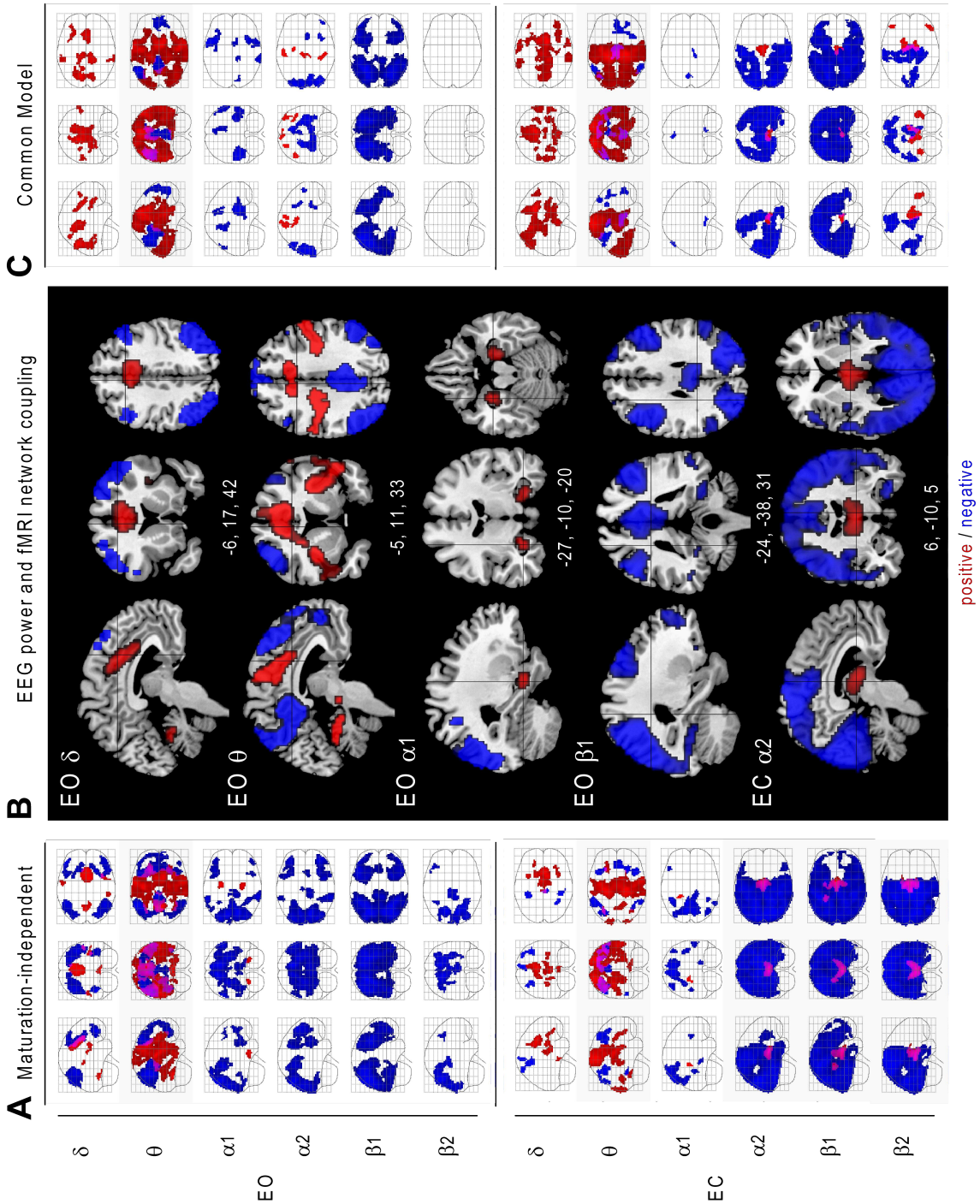

Fig. 2.4 Maturation-independent EEG-BOLD signal correlation results including all 55 participants with age as the covariate. A: Results from the main analysis (separate models). B: Topographical specificity for a selection (entitled accordingly) of the separate models results on anatomical template image (MNI-coordinates specified beneath). C: Maturation-independent partial correlation patterns resulting from the alternative common model analysis. A - C: T-values are shown as maximum intensity projections simultaneously for both positive (red) and negative (blue) correlations. An overlay of red and blue colored voxels in a specific perspective results in pink. Statistical height threshold was set to $p < 0.001$, corrected by extent threshold $k = 25$ voxels.

those found for the same age range with magnetoencephalography, which is insensitive to these changes in physical skull properties (Ciesielski et al., 2010; Puligheddu et al., 2005), corroborates their neurodevelopmental nature.

EEG power maturation was not confined to a local topographical component but indicates changes in diffuse global scalp oscillatory activity as most electrodes were affected. Thus, GSP reflecting the averaged scalp activity captured EEG maturation well. GSP demonstrated that children's activity had more than 4 times higher power values than those found in adults in delta band (1 - 3.5 Hz) and almost 3 times higher in theta band (4 - 7.5 Hz) (Fig. 2.1B). The EEG signal is generated by synaptic activity of synchronized, mainly cortical neuron populations. Although the exact physiological mechanisms of EEG oscillations are not fully understood, their maturational transformation has been found to parallel changes in brain structure (Buchmann et al., 2011; Whitford et al., 2007). The parallel trajectories of EEG amplitudes and gray matter may have a common physiological background, since synaptic density reflects the connectivity and size of neuron populations which EEG amplitudes partly depend on (Boord et al., 2007; Feinberg and Campbell, 2010). In contrast to these former studies, we investigated the relation of EEG maturation to the functional fMRI-BOLD signal.

EEG–BOLD signal correlations

Resting state EEG and fMRI capture two partly complementary aspects of intrinsic brain activity. The brain's intrinsic BOLD activity reveals a spatially segregated functional architecture consisting of coherent large-scale networks (Raichle, 2006). Our data demonstrated a robust coupling between the different EEG oscillations and such networks. Summarized in a maturation-independent analysis we delineated three basic and robust correlation patterns. All three coupling patterns reflect different states of arousal (DMN, ATN) or mechanisms of arousal regulation (TCN). Arousal is likely the dominant factor in spontaneously fluctuating resting state brain activity.

DMN. EO theta was negatively correlated to the DMN, in line with previous findings (Scheeringa et al., 2008). Positive correlations appeared widespread in and near the cinguloopercular network (Dosenbach et al., 2007; Dosenbach et al., 2006). This pattern was similar across both low frequencies in both conditions (as confirmed by inspection at a lower threshold). The inverse relation of theta and DMN is consistent with their association to cognition as theta power (Inanaga, 1998) increases and DMN activity decreases (Raichle and Snyder, 2007) in response to cognitively demanding mental activity. Similarly, the positive correlation between theta and the cinguloopercular network is consistent with its task-positive role (Dosenbach et al., 2007; Dosenbach et al., 2006; Seeley et al., 2007) .

ATN. EO beta1 was negatively correlated in broad occipital and parieto- frontal cortices. The bilateral fronto-parietal pattern, as has been described before (Laufs et al., 2006; Laufs et al., 2003), comprises regions engaged in task processing (Corbetta and Shulman, 2002) and closely matches the ATN found in resting state data (Fox et al., 2005).

TCN. EC alpha oscillations were positively correlated in the thalamus and negatively

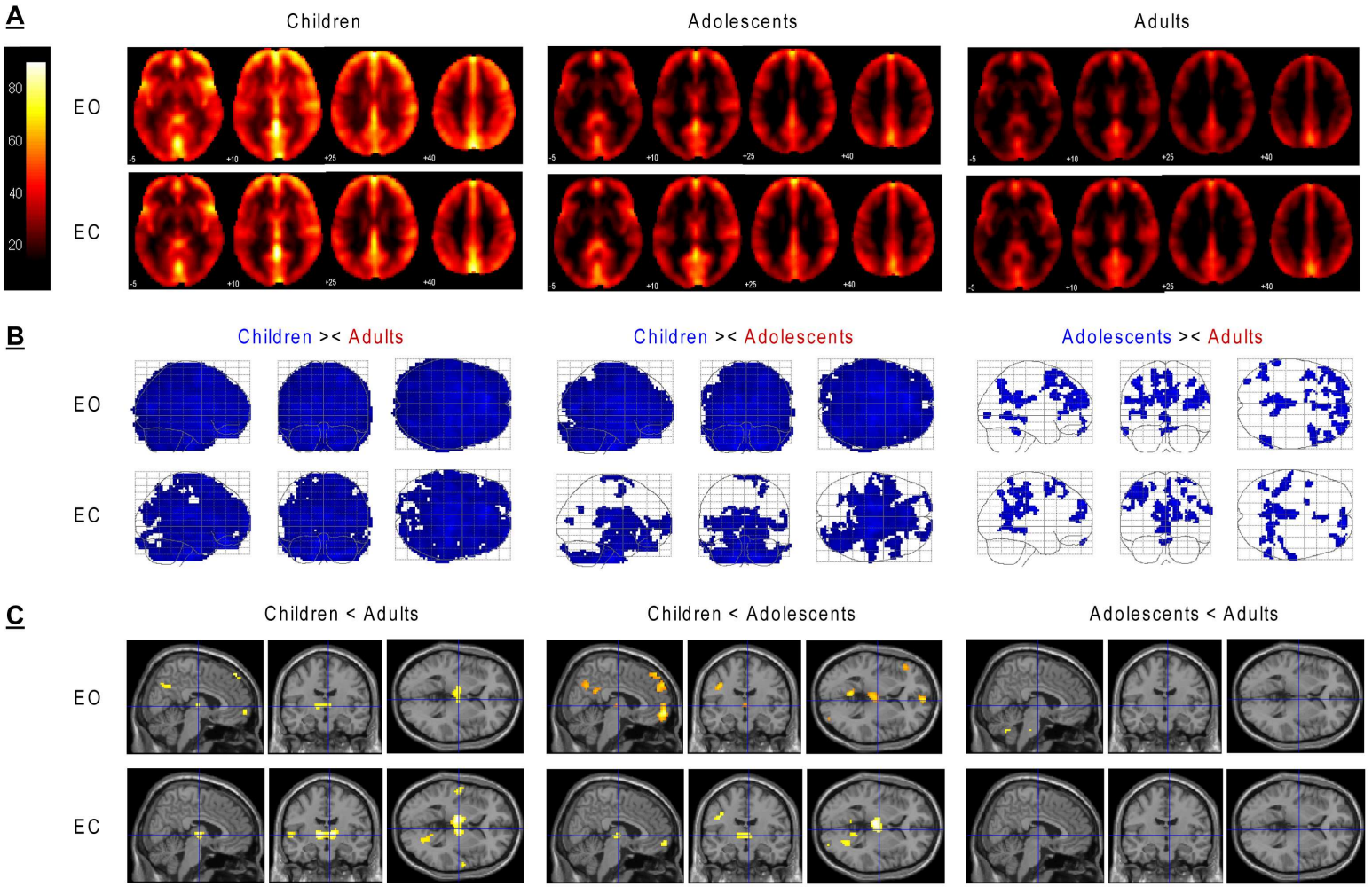

Fig. 2.5 BOLD spectral power analysis. A: Group mean absolute BOLD signal power, separated by condition. Color bar scaling (15 - 90 [arbitrary units]) and slice selection (axial: -5, 10, 25, 40) were kept constant. B: Group differences of absolute BOLD signal power. Contrasts are shown in both directions 'younger <> older' and color-coded as indicated by the column titles. No voxel was observed showing higher BOLD power in the older group. Statistical height threshold was set to $p < 0.001$, corrected by extent threshold $k = 25$ voxels. C: Group differences of normalized BOLD signal power differences separated by condition. T-statistics were superimposed on SPM anatomical template. Slice-coordinates were chosen to highlight the thalamus. Only contrasts 'younger < older' were shown. Statistical height threshold was set to $p < 0.001$, corrected by extent threshold $k = 25$ voxels. The contrast EO 'Children < Adolescents' was thresholded at $p < 0.005$, $k = 25$, to visualize consistency of normalized thalamic power increase with age.

correlated in occipital, parietal and temporal cortex. This replicates the hallmark finding of EEG–fMRI correlations (de Munck et al., 2007; Difrancesco et al., 2008; Feige et al., 2005; Goldman et al., 2002; Goncalves et al., 2006; Lüchinger et al., 2011; Moosmann et al., 2003; Tyvaert et al., 2008) and EEG–PET studies (Sadato et al., 1998; Schreckenberger et al., 2004). This finding corroborates the long standing concept that alpha synchronization reflects an idling state of thalamocortical arousal regulation characterized by cortical down regulation in sensory areas (for review e.g.: Feige et al., 2005). The pattern extended to beta1 and beta2 bands as found before (de Munck et al., 2009; Moosmann et al., 2003). The thalamocortical coupling pattern reported here was not evoked by short-term (e.g. 20 s) alpha reactivity ("Berger effect"), but rather characterizes a more persistent resting state maintenance of 2.5 min.

EO and EC conditions yielded different EEG–BOLD coupling patterns. This suggests that the conditions affect brain function more profoundly than one could expect from the simple blocking of visual input. However, the coupling differences are in line with EEG (Barry et al., 2007; Berger, 1929) and fMRI literature (Bianciardi et al., 2009; Marx et al., 2004; Marx et al., 2003; Yang et al., 2007) reporting EO/EC condition differences. With the increasing interest in resting state brain function, differences between EO and EC have likewise garnered interest, and they also relate to the debate about an optimal 'baseline' (Raichle et al., 2001). The parallel analysis of six major frequency bands ranging from 1 to 30 Hz proofed to be the most important factor influencing the EEG–BOLD correlations. The main effect of frequency was massive and demonstrated that there is substantial variation among frequency bands in spite of the fact that there are moderate inter-frequency dependencies as well. This partly contradicts theoretical models of EEG–fMRI fusion which assume less frequency- and condition-specific transfer functions (Kilner et al., 2005; Rosa et al., 2010).

The band-wise coupling analyses revealed several, at least partly, distinct networks which were both frequency dependent, and varied with arousal states (eyes open versus eyes closed). However, a simple functional interpretation in terms of distinct oscillation speeds of these networks may not be warranted, since we did not examine coupling specifically for the classical fMRI-defined RSN. In addition, coupling with a given frequency does not imply that the network acts as an EEG generator with the given frequency, and the coupling pattern may not converge with the distribution identified by electromagnetic source localization.

Former studies typically used oscillatory activity from a focal component in terms of a subset of electrodes. The robust correlations yielded by GSP suggest that fundamental couplings to DMN, ATN and TCN arise from diffuse rhythms rather than focal components. The previous results for the adult and adolescent groups were replicated using only the first half of the data to equate to the shorter recording duration in children. Such high reliability of the resting EEG–fMRI coupling patterns extends similar findings for separate resting EEG (Buckelmuller et al., 2006; Napflin et al., 2008) and fMRI (Van Dijk et al., 2010) markers.

Common model analysis. Partial correlations were much less frequently reported in the literature (de Munck et al., 2009; Tyvaert et al., 2008), yet explain the portion of

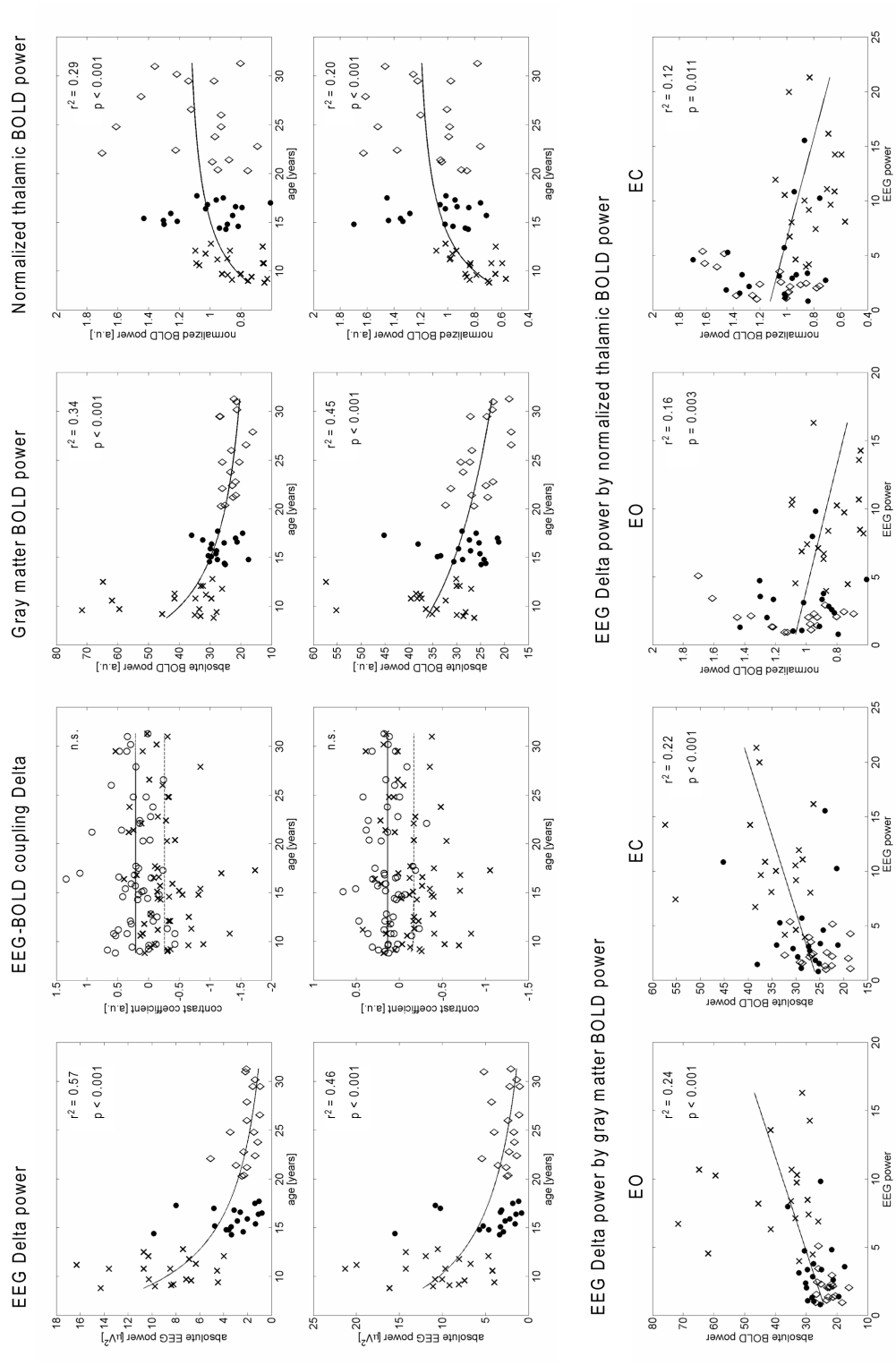

Fig. 2.6 Scatter plots illustrating the main findings. A: EEG power, EEG-BOLD coupling, absolute and normalized BOLD power by age. Markers represent group membership (cross: Children, dot: Adolescents, diamond: Adults). Power curve ($f(x) = a*x^b$) was used for data fit. EEG power and EEG-BOLD coupling is represented by delta band GSP. EEG-BOLD correlations are mean values within significant group mean patterns and are shown for both positive (circle, solid slope) and negative (cross, dashed slope) correlations. Absolute BOLD power was averaged within gray matter voxels (SPM template > 40 %). Normalized BOLD power was averaged within thalamic voxels (AAL-ROI). B: Absolute gray matter and normalized thalamic BOLD power by EEG delta power. Linear slope ($f(x) = a+x*b$) was used for data fit. A and B: coefficients r^2 and p were calculated using SPSS 16.

correlation that is unique to a specific frequency band. Accordingly, DMN correlation is specific to theta power rather than to delta power. ATN correlation is more specific to beta1 than to the neighboring bands and the thalamocortical pattern was specific to all three upper frequency bands alpha2, beta1 and beta2. EC theta manifested a coupling very similar to the thalamocortical pattern, yet with opposite correlation signs. This was not evident in the main analysis. Therefore we interpret these results as mainly model driven effects. The frequency fluctuation changes as non-orthogonal regressors enter the model (Andrade et al., 1999), in this case leaving their fingerprints in concurrent frequency bands.

Maturation of EEG–BOLD coupling patterns

Maturational EEG power attenuation was characterized dominantly by lower frequencies in both conditions and followed a continuous trajectory. We hypothesized that a corresponding substrate of this general power reduction needs to be identifiable in an analog pattern across age, condition and frequency. In contrast, inconsistent effects limited to single factor levels hardly explain the power reduction comprehensively. Despite the fact that the EEG signal at the scalp can be generated in many ways, we further hypothesized that the global vanishing of amplitudes is likely related to profound mechanisms, possibly localized in broad areas across the whole cortex, a large-scale network whose activity affects widespread areas across the brain, or a functionally central region projecting to large portions of the cortex. In contrast, few, small and less centrally integrated regions seem rather implausible.

The EEG–BOLD signal coupling did not change profoundly with maturation as revealed by the ANOVA main effect of age. Although the coupling differed significantly in the right visual cortex, this focal, peripheral cluster did not match our scheme to possibly account for global EEG change. The group differences in EEG–BOLD coupling (Fig. 2.3B) revealed no consistent pattern of changes. The few significant differences were neither focused on low frequencies nor did they reoccur between the groups contrasts, which would indicate a continuous maturational track similar to EEG. A consistent meaningful pattern across group, condition and frequency was not identified at very low statistical threshold either. This is important as the power attenuation may be very loosely related to changing correlated activity in brain regions. The lack of a direct correspondence between changing EEG power and retaining EEG–BOLD signal correlations means that the fluctuations driving these correlations are largely independent from the oscillatory magnitude in the EEG signal. The correlation measure reflects the coherence of signal time courses independent from the scales. Therefore, the amplitudes depending on neuronal masses are likely independent from synaptic pruning. The functional coupling reflects a distinct aspect of neurophysiological activity that presumably matures earlier than the neurodevelopmental process responsible for low frequency EEG attenuation. These results are consistent with similar findings in our previous report on late maturation (Lüchinger et al., 2011). EEG oscillations were coupled to RSN's such as the DMN. The significant EEG coupling to these RSNs even at the age of 8 years is plausible as RSN's were found to be established already at the age of 7 - 9 years (Fair et al., 2009; Fair et al., 2007;

Supekar et al., 2009). Our results thus suggest that EEG oscillations of a given frequency keep the same connotation between children and adults in terms of functional correlate to BOLD signal activity, and that most frequency specific BOLD topographies are conserved across development despite changes in EEG frequency composition.

Although we did not find a 'direct' correspondence, we identified robust age-related differences in the thalamocortical coupling pattern. This key feature of EEG–BOLD coupling differed between children and adolescents as well as children and adults significantly in terms of less negative cortical and less positive thalamic correlations. Children did not indicate a coupling of EEG fluctuation to thalamic activity at all (Fig. 2.3A), even at very low statistical threshold. The thalamocortical pattern associated with EC alpha2, beta1 and beta2 matures between the ages of 10 to 16 years. This suggests that the depicted oscillations have a different connotation in children than in adolescents or adults, as their functional coupling to BOLD signal activity is significantly different.

Although this EEG–BOLD coupling maturation was limited to EC higher frequencies, it is tempting to speculate about an 'indirect' relation to the dominantly low frequency power decrease, due to the fundamental role of the thalamus and thalamocortical circuitry for brain state regulation and the generation of scalp electric oscillations. The higher frequency EC correlation to thalamocortical BOLD signal does not imply that the thalamus and thalamocoritcal interaction itself oscillates in this particular frequency range only during EC. Thalamic and thalamocortcial state regulation feature other frequency ranges and are well known to be related to low frequency scalp activity (Brandeis et al., 2009). EEG maturation therefore may be related to thalamic and thalamocortical activity as well. The higher frequency EC EEG–BOLD coupling may reflect only a distinct aspect and small portion of thalamocortical activity limited to state- and frequency-dependent scalp activity. Nevertheless, it yielded the functional maturation in these structures with converging evidence from normalized BOLD power, thus indicating state-independent thalamic maturation (see below). Hence we propose that EEG power decrease may be 'indirectly' related to higher frequency EC EEG–BOLD coupling changes as they could emerge from the same neuronal substrate (the maturational changes in thalamocortical activity). However, (low frequency) EEG power decrease and thalamocortical changes may also be independent phenomena of brain maturation.

This proposal would link brain maturation with other brain states based on the converging feature of low frequency excess, for which the thalamus and thalamocortical circuits are well-established neuronal substrates. Such states are low arousal states like sleep (Steriade et al., 1993; Tsai et al., 2010) or anesthesia (John et al., 2001), and neuropathology (Llinas et al., 1999; Michels et al., 2011a; Michels et al., 2011b; Sarnthein et al., 2003). Low arousal states and neuropathologic conditions can be seen as states of lower brain functioning. Our results suggest that brain immaturity resembles features of lower brain functioning as well. The result is also in line with findings that some EEG and fMRI markers implicate a maturational lag in neurodevelopmental disorders such as Attention Deficit Hyperactivity Disorder (Doehnert et al., 2010; Fair et al., 2010), but

by no means implies that normal immaturity in childhood represents a pathological or under-aroused state.

The EEG–BOLD coupling results might be partly influenced by age-related confounds in physiological noise, such as breathing (which we did not record) or blood-pulse artifact. In developmental EEG and fMRI studies breathing is rarely accounted for. In simultaneous EEG–fMRI the main physiological confound comes from motion-related blood-pulse artifact due to magnetic field strength (Debener et al., 2008). The procedure for blood-pulse artifact reduction was standardized and carefully applied to all groups in the same way. Younger participants tend to have a higher pulse rate, but the performance of the average artifact subtraction is not influenced by the pulse rate. The same BCG artifact ICA components were rejected between the groups as the topography as well as the frequency pattern does not change across age groups. In addition, the number of excluded ICA components which contained residual EEG artifacts did not differ between children and adolescents. Since the major developmental effects on EEG and EEG–BOLD coupling were observed between these two groups, a contribution of differences in EEG quality is thus unlikely. Based on the EEG results shown in Figure 1A and B we conclude that the pulse artifact reduction was well achieved. Some remaining BCG artifact can be seen in the group mean topography but the group differences do not indicate a systematic bias with age.

We describe group differences in EEG–BOLD coupling state dependent in higher (> 10 Hz). The BCG artifact is strongest between 0 and 4 Hz. Group differences caused by confounding BCG artifact would (i) produce group differences in lower frequencies and (ii) affect both resting states similarly, as the age related pulse differences are state-independent. Importantly, the coupling pattern in low frequencies (delta, theta) did not differ between children and older participants. For example the components of the DMN or the cingulo-opercular network appeared in all groups in delta/theta. It would be difficult to explain why remaining BCG would affect the EC high frequency range but not state independent low frequency range. Nevertheless we cannot exclude by definition that the lacking thalamocortical coupling pattern in children could be influenced by remaining BCG contamination. Future studies might include approaches to better account for physiological confounds (Glover et al., 2000).

Maturation of the magnitude of spontaneous BOLD signal fluctuations

BOLD signal power was calculated for a direct comparison to EEG power maturation in terms of equivalent measures. The spontaneous fluctuating BOLD signal reflects the energy demand of the brain at rest (Raichle, 2006). The BOLD signal power was averaged within the low frequency range (0.01 - 0.08 Hz) which drives the functional connectivity and the RSNs, and which is believed to reflect mainly neuronal activity. Our data revealed prominent, global activity decrease in the resting BOLD signal with age (Fig. 2.5B). Strongest in children, the BOLD signal trajectory followed a non-linear decrease very similar to low frequency EEG power (Fig. 2.6A). To our knowledge, this finding is novel and provides a new marker for functional brain maturation. The decrease in hemodynamic

rest activity relates to other markers of structural and functional brain maturation that show similar decreases during adolescence (Boord et al., 2007; Feinberg and Campbell, 2010; Feinberg et al., 1990). The hemodynamic activity fluctuation attenuation also parallels the structural and metabolic maturation spatially, as a global phenomenon, affecting the entire brain. Possibly, the hemodynamic power decrease is coupled with metabolic decrease (Biagi et al., 2007; Chugani, 1998; Chugani et al., 1987; Taki et al., 2011), and both decreases may be guided by synaptic pruning (Giedd et al., 1999; Gogtay et al., 2004; Huttenlocher, 1979). Even if the physiological coupling between the diverse measures is not fully understood, the pattern represents converging evidence for general functional and structural reorganization towards higher efficiency.

The subtraction of the individual mean power level was expected to increase the sensitivity to spatial differences at the cost of sensitivity to global amplitude reductions with maturation. Since this normalized BOLD power was typically used in previous studies, these results connect most directly to the literature. After this normalization the relative BOLD activity was found to increase with age in the thalamus (Fig. 2.5C). This demonstrated the high functional specificity of BOLD signal power measure and directly corresponded to the maturation in the thalamocortical EEG–BOLD coupling. The normalized thalamic BOLD power correlated to the thalamic EC alpha2-BOLD coupling with $r = 0.557$ across participants in a post-hoc calculation. As noted above, this relative activity increase in the thalamus, together with the immature thalamocortical EEG–BOLD coupling provides converging evidence for maturational change in thalamocortical brain state regulation during rest. The thalamic and thalamocortical functions associated with abilities to transiently disconnect from environmental input, regulate sensory or motor distraction, and the maintenance of prolonged mental focus characterize human behavioral maturation.

Conventional fMRI studies report both increases as well as decreases in local BOLD activity as maturational correlate of cognitive functions (Blakemore and Choudhury, 2006), depending on the specific task, brain region and developmental phase. However interpretations of maturational BOLD signal chances are hampered by confounding factors such as cognitive effort, experience and strategy (Casey et al., 2005). Although our results need to be verified in further studies, the resting state BOLD power provides an absolute quantity of functional brain maturation and is less ambiguous in terms of behavioral confounds. Although the BOLD signal power was analyzed in the spectral range thought to reflect neuronal activity (< 0.1 Hz), physiological confounds such as respiration and blood pulse in the higher frequency range (> 0.1 Hz) can affect lower frequency ranges by aliasing (Birn et al., 2008). The spatial patterns of both absolute and normalized BOLD signal power maturation were different from those typically yielded by physiological artifacts.

We hypothesize that these BOLD power decreases with age are related to the gray matter volume decreases, similar to the maturational decreases of slow EEG activity (Whitford et al., 2007) which remain correlated with gray matter reductions even after correcting for whole-brain volume (Buchmann et al., 2011). Therefore, we interpret our results as mainly driven by neuronal maturation, although this needs to be confirmed in

further studies.

Conclusion

This study demonstrates that global EEG low frequency power decrease from childhood to adulthood (8.8 - 31.3 years) is paralleled by global BOLD signal power decrease, while temporal functional coupling remains largely unchanged. The novel finding of global BOLD signal power decrease is consistent with global decreases in structural and metabolic markers, indicating profound neuronal reorganization during adolescence. Moreover, thalamic and thalamocortical maturation was implicated by EEG–fMRI coupling and normalized BOLD power.

Acknowledgements

This work was supported by the University Research Priority Program "Integrative Human Physiology" at the University of Zurich. We are grateful for all the participant interest in the study; we especially thank the children and their parents for their commitment.

References

Allen, P.J., Josephs, O., Turner, R., 2000. A method for removing imaging artifact from continuous EEG recorded during functional MRI. Neuroimage 12, 230-239.

Allen, P.J., Polizzi, G., Krakow, K., Fish, D.R., Lemieux, L., 1998. Identification of EEG events in the MR scanner: the problem of pulse artifact and a method for its subtraction. Neuroimage 8, 229-239.

Andrade, A., Paradis, A.L., Rouquette, S., Poline, J.B., 1999. Ambiguous results in functional neuroimaging data analysis due to covariate correlation. Neuroimage 10, 483-486.

Baria, A.T., Baliki, M.N., Parrish, T., Apkarian, A.V., 2011. Anatomical and Functional Assemblies of Brain BOLD Oscillations. J Neurosci 31, 7910-7919.

Barry, R.J., Clarke, A.R., Johnstone, S.J., Brown, C.R., 2009. EEG differences in children between eyes-closed and eyes-open resting conditions. Clin Neurophysiol 120, 1806-1811.

Barry, R.J., Clarke, A.R., Johnstone, S.J., Magee, C.A., Rushby, J.A., 2007. EEG differences between eyes-closed and eyes-open resting conditions. Clin Neurophysiol 118, 2765-2773.

Berger, H., 1929 Über das Elektrenkephalogramm des Menschen. European Archives of Psychiatry and Clinical Neuroscience 87, 527-570.

Biagi, L., Abbruzzese, A., Bianchi, M.C., Alsop, D.C., Del Guerra, A., Tosetti, M., 2007. Age dependence of cerebral perfusion assessed by magnetic resonance continuous arterial spin labeling. J Magn Reson Imaging 25, 696-702.

Bianciardi, M., Fukunaga, M., van Gelderen, P., Horovitz, S.G., de Zwart, J.A., Duyn, J.H., 2009. Modulation of spontaneous fMRI activity in human visual cortex by behavioral state. Neuroimage 45, 160-168.

Birn, R.M., Murphy, K., Bandettini, P.A., 2008. The effect of respiration variations on independent component analysis results of resting state functional connectivity. Hum Brain Mapp 29, 740-750.

Biswal, B., Yetkin, F.Z., Haughton, V.M., Hyde, J.S., 1995. Functional connectivity in the motor cortex of resting human brain using echo-planar MRI. Magn Reson Med 34, 537-541.

Biswal, B.B., Mennes, M., Zuo, X.N., Gohel, S., Kelly, C., Smith, S.M., Beckmann, C.F., Adelstein, J.S., Buckner, R.L., Colcombe, S., Dogonowski, A.M., Ernst, M., Fair, D., Hampson, M., Hoptman, M.J., Hyde, J.S., Kiviniemi, V.J., Kotter, R., Li, S.J., Lin, C.P., Lowe, M.J., Mackay, C., Madden, D.J., Madsen, K.H., Margulies, D.S., Mayberg, H.S., McMahon, K., Monk, C.S., Mostofsky, S.H., Nagel, B.J., Pekar, J.J., Peltier, S.J., Petersen, S.E., Riedl, V., Rombouts, S.A., Rypma, B., Schlaggar, B.L., Schmidt, S., Seidler, R.D., Siegle, G.J., Sorg, C., Teng, G.J., Veijola, J., Villringer, A., Walter, M., Wang, L., Weng, X.C., Whitfield-Gabrieli, S.,

Williamson, P., Windischberger, C., Zang, Y.F., Zhang, H.Y., Castellanos, F.X., Milham, M.P., 2010. Toward discovery science of human brain function. Proc Natl Acad Sci U S A 107, 4734-4739.

Blakemore, S.J., Choudhury, S., 2006. Brain development during puberty: state of the science. Dev Sci 9, 11-14.

Boord, P.R., Rennie, C.J., Williams, L.M., 2007. Integrating "brain" and "body" measures: correlations between EEG and metabolic changes over the human lifespan. J Integr Neurosci 6, 205-218.

Bourgeois, J.P., Rakic, P., 1993. Changes of synaptic density in the primary visual cortex of the macaque monkey from fetal to adult stage. J Neurosci 13, 2801-2820.

Brandeis, D., Michel, M.C., Amzica, F., 2009. From neuronal activity to scalp potential fields. In: Michel, M.C., Koenig, T., Brandeis, D., Gianotti, L.R.R., Wackermann, J. (Eds.), Electrical Neuroimaging. Cambridge Unversity Press, New York, pp. 1-24.

Brown, T.T., Petersen, S.E., Schlaggar, B.L., 2006. Does human functional brain organization shift from diffuse to focal with development? Dev Sci 9, 9-11.

Buchmann, A., Ringli, M., Kurth, S., Schaerer, M., Geiger, A., Jenni, O.G., Huber, R., 2011. EEG sleep slow-wave activity as a mirror of cortical maturation. Cereb Cortex 21, 607-615.

Buckelmuller, J., Landolt, H.P., Stassen, H.H., Achermann, P., 2006. Trait-like individual differences in the human sleep electroencephalogram. Neuroscience 138, 351-356.

Cajochen, C., Wyatt, J.K., Czeisler, C.A., Dijk, D.J., 2002. Separation of circadian and wake duration-dependent modulation of EEG activation during wakefulness. Neuroscience 114, 1047-1060.

Calhoun, V.D., Kiehl, K.A., Pearlson, G.D., 2008. Modulation of temporally coherent brain networks estimated using ICA at rest and during cognitive tasks. Hum Brain Mapp 29, 828-838.

Campbell, I.G., Feinberg, I., 2009. Longitudinal trajectories of non-rapid eye movement delta and theta EEG as indicators of adolescent brain maturation. Proc Natl Acad Sci U S A 106, 5177-5180.

Case, R., 1992. The role of the frontal lobes in the regulation of cognitive development. Brain Cogn 20, 51-73. Casey, B.J., Galvan, A., Hare, T.A., 2005. Changes in cerebral functional organization during cognitive development. Curr Opin Neurobiol 15, 239-244.

Chugani, H.T., 1998. A critical period of brain development: studies of cerebral glucose utilization with PET. Prev Med 27, 184-188.

Chugani, H.T., Phelps, M.E., Mazziotta, J.C., 1987. Positron emission tomography study of human brain functional development. Ann Neurol 22, 487-497.

Ciesielski, K.T., Ahlfors, S.P., Bedrick, E.J., Kerwin, A.A., Hamalainen, M.S., 2010. Top-down control of MEG alpha-band activity in children performing Categorical N-Back Task. Neuropsychologia 48, 3573-3579.

Corbetta, M., Shulman, G.L., 2002. Control of goal-directed and stimulus-driven attention in the brain. Nat Rev Neurosci 3, 201-215.

Cordes, D., Haughton, V.M., Arfanakis, K., Carew, J.D., Turski, P.A., Moritz, C.H., Quigley, M.A., Meyerand, M.E., 2001. Frequencies contributing to functional connectivity in the cerebral cortex in "resting-state" data. AJNR Am J Neuroradiol 22, 1326-1333.

Cowan, W.M., Fawcett, J.W., O'Leary, D.D., Stanfield, B.B., 1984. Regressive events in neurogenesis. Science 225, 1258-1265.

Damoiseaux, J.S., Rombouts, S.A., Barkhof, F., Scheltens, P., Stam, C.J., Smith, S.M., Beckmann, C.F., 2006. Consistent resting-state networks across healthy subjects. Proc Natl Acad Sci U S A 103, 13848-13853.

de Munck, J.C., Goncalves, S.I., Huijboom, L., Kuijer, J.P., Pouwels, P.J., Heethaar, R.M., Lopes da Silva, F.H., 2007. The hemodynamic response of the alpha rhythm: an EEG/fMRI study. Neuroimage 35, 1142-1151.

de Munck, J.C., Goncalves, S.I., Mammoliti, R., Heethaar, R.M., Lopes da Silva, F.H., 2009. Interactions between different EEG frequency bands and their effect on alpha-fMRI correlations. Neuroimage 47, 69-76.

Debener, S., Mullinger, K.J., Niazy, R.K., Bowtell, R.W., 2008. Properties of the ballistocardiogram artefact as revealed by EEG recordings at 1.5, 3 and 7 T static magnetic field strength. Int J Psychophysiol 67, 189-199.

Deco, G., Jirsa, V.K., McIntosh, A.R., 2011. Emerging concepts for the dynamical organization of resting-state activity in the brain. Nat Rev Neurosci 12, 43-56.

Delorme, A., Makeig, S., 2004. EEGLAB: an open source toolbox for analysis of single-trial EEG dynamics including independent component analysis. J Neurosci Methods 134, 9-21.

Dick, F., Leech, R., Moses, P., Saccuman, M.C., 2006. The interplay of learning and development in shaping neural organization. Dev Sci 9, 14-17.

Difrancesco, M.W., Holland, S.K., Szaflarski, J.P., 2008. Simultaneous EEG/functional magnetic resonance imaging at 4 Tesla: correlates of brain activity to spontaneous alpha rhythm during relaxation. J Clin Neurophysiol 25, 255-264.

Doehnert, M., Brandeis, D., Imhof, K., Drechsler, R., Steinhausen, H.C., 2010. Mapping attention-deficit/hyperactivity disorder from childhood to adolescence–no neurophysiologic evidence for a developmental lag of attention but

some for inhibition. Biol Psychiatry 67, 608-616.
Dosenbach, N.U., Fair, D.A., Miezin, F.M., Cohen, A.L., Wenger, K.K., Dosenbach, R.A., Fox, M.D., Snyder, A.Z., Vincent, J.L., Raichle, M.E., Schlaggar, B.L., Petersen, S.E., 2007. Distinct brain networks for adaptive and stable task control in humans. Proc Natl Acad Sci U S A 104, 11073-11078.
Dosenbach, N.U., Nardos, B., Cohen, A.L., Fair, D.A., Power, J.D., Church, J.A., Nelson, S.M., Wig, G.S., Vogel, A.C., Lessov-Schlaggar, C.N., Barnes, K.A., Dubis, J.W., Feczko, E., Coalson, R.S., Pruett, J.R., Jr., Barch, D.M., Petersen, S.E., Schlaggar, B.L., 2010. Prediction of individual brain maturity using fMRI. Science 329, 1358-1361.
Dosenbach, N.U., Visscher, K.M., Palmer, E.D., Miezin, F.M., Wenger, K.K., Kang, H.C., Burgund, E.D., Grimes, A.L., Schlaggar, B.L., Petersen, S.E., 2006. A core system for the implementation of task sets. Neuron 50, 799-812.
Duff, E.P., Johnston, L.A., Xiong, J., Fox, P.T., Mareels, I., Egan, G.F., 2008. The power of spectral density analysis for mapping endogenous BOLD signal fluctuations. Hum Brain Mapp 29, 778-790.
Durston, S., Davidson, M.C., Tottenham, N., Galvan, A., Spicer, J., Fossella, J.A., Casey, B.J., 2006. A shift from diffuse to focal cortical activity with development. Dev Sci 9, 1-8.
Dustman, R.E., Shearer, D.E., Emmerson, R.Y., 1999. Life-span changes in EEG spectral amplitude, amplitude variability and mean frequency. Clin Neurophysiol 110, 1399-1409.
Eeg-Olofsson, O., 1970. The development of the electroencephalogram in normal children and adolescents from the age of 1 through 21 years. Acta Paediatr Scand Suppl 208, Suppl208:201+.
Fair, D.A., Cohen, A.L., Power, J.D., Dosenbach, N.U., Church, J.A., Miezin, F.M., Schlaggar, B.L., Petersen, S.E., 2009. Functional brain networks develop from a "local to distributed" organization. PLoS Comput Biol 5, e1000381.
Fair, D.A., Dosenbach, N.U., Church, J.A., Cohen, A.L., Brahmbhatt, S., Miezin, F.M., Barch, D.M., Raichle, M.E., Petersen, S.E., Schlaggar, B.L., 2007. Development of distinct control networks through segregation and integration. Proc Natl Acad Sci U S A 104, 13507-13512.
Fair, D.A., Posner, J., Nagel, B.J., Bathula, D., Dias, T.G., Mills, K.L., Blythe, M.S., Giwa, A., Schmitt, C.F., Nigg, J.T., 2010. Atypical default network connectivity in youth with attention-deficit/hyperactivity disorder. Biol Psychiatry 68, 1084-1091.
Feige, B., Scheffler, K., Esposito, F., Di Salle, F., Hennig, J., Seifritz, E., 2005. Cortical and subcortical correlates of electroencephalographic alpha rhythm modulation. J Neurophysiol 93, 2864-2872.
Feinberg, I., Campbell, I.G., 2010. Sleep EEG changes during adolescence: an index of a fundamental brain reorganization. Brain Cogn 72, 56-65.
Feinberg, I., Thode, H.C., Jr., Chugani, H.T., March, J.D., 1990. Gamma distribution model describes maturational curves for delta wave amplitude, cortical metabolic rate and synaptic density. J Theor Biol 142, 149-161.
Forman, S.D., Cohen, J.D., Fitzgerald, M., Eddy, W.F., Mintun, M.A., Noll, D.C., 1995. Improved assessment of significant activation in functional magnetic resonance imaging (fMRI): use of a cluster-size threshold. Magn Reson Med 33, 636-647.
Fox, M.D., Raichle, M.E., 2007. Spontaneous fluctuations in brain activity observed with functional magnetic resonance imaging. Nat Rev Neurosci 8, 700-711.
Fox, M.D., Snyder, A.Z., Vincent, J.L., Corbetta, M., Van Essen, D.C., Raichle, M.E., 2005. The human brain is intrinsically organized into dynamic, anticorrelated functional networks. Proc Natl Acad Sci U S A 102, 9673-9678.
Friston, K., 2002. Beyond phrenology: what can neuroimaging tell us about distributed circuitry? Annu Rev Neurosci 25, 221-250.
Gasser, T., Verleger, R., Bacher, P., Sroka, L., 1988. Development of the EEG of school-age children and adolescents. I. Analysis of band power. Electroencephalogr Clin Neurophysiol 69, 91-99. Gibbs, F.A., Knott, J.R., 1949. Growth of the electrical activity of the cortex. Electroencephalogr Clin Neurophysiol 1, 223-229.
Giedd, J.N., Blumenthal, J., Jeffries, N.O., Castellanos, F.X., Liu, H., Zijdenbos, A., Paus, T., Evans, A.C., Rapoport, J.L., 1999. Brain development during childhood and adolescence: a longitudinal MRI study. Nat Neurosci 2, 861-863.
Glover, G.H., Li, T.Q., Ress, D., 2000. Image-based method for retrospective correction of physiological motion effects in fMRI: RETROICOR. Magn Reson Med 44, 162-167.
Gogtay, N., Giedd, J.N., Lusk, L., Hayashi, K.M., Greenstein, D., Vaituzis, A.C., Nugent, T.F., 3rd, Herman, D.H., Clasen, L.S., Toga, A.W., Rapoport, J.L., Thompson, P.M., 2004. Dynamic mapping of human cortical development during childhood through early adulthood. Proc Natl Acad Sci U S A 101, 8174-8179.
Gogtay, N., Thompson, P.M., 2010. Mapping gray matter development: implications for typical development and vulnerability to psychopathology. Brain Cogn 72, 6-15.
Goldman, R.I., Stern, J.M., Engel, J., Jr., Cohen, M.S., 2002. Simultaneous EEG and fMRI of the alpha rhythm. Neuroreport 13, 2487-2492.

Goncalves, S.I., de Munck, J.C., Pouwels, P.J., Schoonhoven, R., Kuijer, J.P., Maurits, N.M., Hoogduin, J.M., Van Someren, E.J., Heethaar, R.M., Lopes da Silva, F.H., 2006. Correlating the alpha rhythm to BOLD using simultaneous EEG/fMRI: inter-subject variability. Neuroimage 30, 203-213.

Gusnard, D.A., Raichle, M.E., 2001. Searching for a baseline: functional imaging and the resting human brain. Nat Rev Neurosci 2, 685-694.

Hoekema, R., Wieneke, G.H., Leijten, F.S., van Veelen, C.W., van Rijen, P.C., Huiskamp, G.J., Ansems, J., van Huffelen, A.C., 2003. Measurement of the conductivity of skull, temporarily removed during epilepsy surgery. Brain Topogr 16, 29-38.

Horovitz, S.G., Fukunaga, M., de Zwart, J.A., van Gelderen, P., Fulton, S.C., Balkin, T.J., Duyn, J.H., 2008. Low frequency BOLD fluctuations during resting wakefulness and light sleep: a simultaneous EEG–fMRI study. Hum Brain Mapp 29, 671-682.

Huttenlocher, P.R., 1979. Synaptic density in human frontal cortex - developmental changes and effects of aging. Brain Res 163, 195-205.

Inanaga, K., 1998. Frontal midline theta rhythm and mental activity. Psychiatry Clin Neurosci 52, 555-566. Jann, K., Dierks, T., Boesch, C., Kottlow, M., Strik, W., Koenig, T., 2009. BOLD correlates of EEG alpha phase-locking and the fMRI default mode network. Neuroimage 45, 903-916.

John, E.R., Ahn, H., Prichep, L., Trepetin, M., Brown, D., Kaye, H., 1980. Developmental equations for the electroencephalogram. Science 210, 1255-1258.

John, E.R., Prichep, L.S., Kox, W., Valdes-Sosa, P., Bosch-Bayard, J., Aubert, E., Tom, M., di Michele, F., Gugino, L.D., 2001. Invariant reversible QEEG effects of anesthetics. Conscious Cogn 10, 165-183.

Jolles, D.D., van Buchem, M.A., Crone, E.A., Rombouts, S.A., 2011. A comprehensive study of whole-brain functional connectivity in children and young adults. Cereb Cortex 21, 385-391.

Jung, T.P., Makeig, S., Westerfield, M., Townsend, J., Courchesne, E., Sejnowski, T.J., 2000. Removal of eye activity artifacts from visual event-related potentials in normal and clinical subjects. Clin Neurophysiol 111, 1745-1758.

Kilner, J.M., Mattout, J., Henson, R., Friston, K.J., 2005. Hemodynamic correlates of EEG: a heuristic. Neuroimage 28, 280-286.

Klimesch, W., 1999. EEG alpha and theta oscillations reflect cognitive and memory performance: a review and analysis. Brain Res Brain Res Rev 29, 169-195.

Kurth, S., Ringli, M., Geiger, A., LeBourgeois, M., Jenni, O.G., Huber, R., 2010. Mapping of cortical activity in the first two decades of life: a high-density sleep electroencephalogram study. J Neurosci 30, 13211-13219.

Laufs, H., Holt, J.L., Elfont, R., Krams, M., Paul, J.S., Krakow, K., Kleinschmidt, A., 2006. Where the BOLD signal goes when alpha EEG leaves. Neuroimage 31, 1408-1418.

Laufs, H., Kleinschmidt, A., Beyerle, A., Eger, E., Salek-Haddadi, A., Preibisch, C., Krakow, K., 2003. EEG–correlated fMRI of human alpha activity. Neuroimage 19, 1463-1476.

Lehmann, D., Skrandies, W., 1980. Reference-free identification of components of checkerboard-evoked multichannel potential fields. Electroencephalogr Clin Neurophysiol 48, 609-621.

Llinas, R., Ribary, U., Contreras, D., Pedroarena, C., 1998. The neuronal basis for consciousness. Philos Trans R Soc Lond B Biol Sci 353, 1841-1849.

Llinas, R., Urbano, F.J., Leznik, E., Ramirez, R.R., van Marle, H.J., 2005. Rhythmic and dysrhythmic thalamocortical dynamics: GABA systems and the edge effect. Trends Neurosci 28, 325-333.

Llinas, R.R., Ribary, U., Jeanmonod, D., Kronberg, E., Mitra, P.P., 1999. Thalamocortical dysrhythmia: A neurological and neuropsychiatric syndrome characterized by magnetoencephalography. Proc Natl Acad Sci U S A 96, 15222-15227.

Logothetis, N.K., Pauls, J., Augath, M., Trinath, T., Oeltermann, A., 2001. Neurophysiological investigation of the basis of the fMRI signal. Nature 412, 150-157.

Lüchinger, R., Michels, L., Martin, E., Brandeis, D., 2011. EEG–BOLD correlations during (post-)adolescent brain maturation. Neuroimage 56, 1493-1505.

Marx, E., Deutschlander, A., Stephan, T., Dieterich, M., Wiesmann, M., Brandt, T., 2004. Eyes open and eyes closed as rest conditions: impact on brain activation patterns. Neuroimage 21, 1818-1824.

Marx, E., Stephan, T., Nolte, A., Deutschlander, A., Seelos, K.C., Dieterich, M., Brandt, T., 2003. Eye closure in darkness animates sensory systems. Neuroimage 19, 924-934.

Matousek, M., Petersen, I., 1973. Automatic evaluation of EEG background activity by means of age-dependent EEG quotients. Electroencephalogr Clin Neurophysiol 35, 603-612.

Matsuura, M., Yamamoto, K., Fukuzawa, H., Okubo, Y., Uesugi, H., Moriiwa, M., Kojima, T., Shimazono, Y., 1985. Age development and sex differences of various EEG elements in healthy children and adults–quantification by a computerized wave form recognition method. Electroencephalogr Clin Neurophysiol 60, 394-406.

McCormick, D.A., Bal, T., 1997. Sleep and arousal: thalamocortical mechanisms. Annu Rev Neurosci 20, 185-215.

Mennes, M., Kelly, C., Zuo, X.N., Di Martino, A., Biswal, B.B., Castellanos, F.X., Milham, M.P., 2010. Inter-individual differences in resting-state functional connectivity predict task-induced BOLD activity. Neuroimage 50, 1690-1701.

Michels, L., Bucher, K., Brem, S., Halder, P., Lüchinger, R., Liechti, M., Martin, E., Jeanmonod, D., Kroll, J., Brandeis, D., 2011a. Does Greater Low Frequency EEG Activity in Normal Immaturity and in Children with Epilepsy Arise in the Same Neuronal Network? Brain Topogr 5, 78-89.

Michels, L., Bucher, K., Lüchinger, R., Klaver, P., Martin, E., Jeanmonod, D., Brandeis, D., 2010. Simultaneous EEG–fMRI during a working memory task: modulations in low and high frequency bands. PLoS One 5, e10298.

Michels, L., Moazami-Goudarzi, M., Jeanmonod, D., 2011b. Correlations between EEG and clinical outcome in chronic neuropathic pain: surgical effects and treatment resistance. Brain Imaging And Behavior 5, 329-348.

Moosmann, M., Ritter, P., Krastel, I., Brink, A., Thees, S., Blankenburg, F., Taskin, B., Obrig, H., Villringer, A., 2003. Correlates of alpha rhythm in functional magnetic resonance imaging and near infrared spectroscopy. Neuroimage 20, 145-158.

Napflin, M., Wildi, M., Sarnthein, J., 2008. Test-retest reliability of EEG spectra during a working memory task. Neuroimage 43, 687-693.

Niessing, J., Ebisch, B., Schmidt, K.E., Niessing, M., Singer, W., Galuske, R.A., 2005. Hemodynamic signals correlate tightly with synchronized gamma oscillations. Science 309, 948-951.

Nir, Y., Fisch, L., Mukamel, R., Gelbard-Sagiv, H., Arieli, A., Fried, I., Malach, R., 2007. Coupling between neuronal firing rate, gamma LFP, and BOLD fMRI is related to interneuronal correlations. Curr Biol 17, 1275-1285.

Olbrich, S., Mulert, C., Karch, S., Trenner, M., Leicht, G., Pogarell, O., Hegerl, U., 2009. EEG–vigilance and BOLD effect during simultaneous EEG/fMRI measurement. Neuroimage 45, 319-332.

Oldfield, R.C., 1971. The assessment and analysis of handedness: the Edinburgh inventory. Neuropsychologia 9, 97-113.

Paus, T., Keshavan, M., Giedd, J.N., 2008. Why do many psychiatric disorders emerge during adolescence? Nat Rev Neurosci 9, 947-957.

Puligheddu, M., de Munck, J.C., Stam, C.J., Verbunt, J., de Jongh, A., van Dijk, B.W., Marrosu, F., 2005. Age distribution of MEG spontaneous theta activity in healthy subjects. Brain Topogr 17, 165-175.

Raichle, M.E., 2006. Neuroscience. The brain's dark energy. Science 314, 1249-1250.

Raichle, M.E., MacLeod, A.M., Snyder, A.Z., Powers, W.J., Gusnard, D.A., Shulman, G.L., 2001. A default mode of brain function. Proc Natl Acad Sci U S A 98, 676-682.

Raichle, M.E., Snyder, A.Z., 2007. A default mode of brain function: a brief history of an evolving idea. Neuroimage 37, 1083-1090; discussion 1097-1089.

Rosa, M.J., Kilner, J., Blankenburg, F., Josephs, O., Penny, W., 2010. Estimating the transfer function from neuronal activity to BOLD using simultaneous EEG–fMRI. Neuroimage 49, 1496-1509.

Sadaghiani, S., Scheeringa, R., Lehongre, K., Morillon, B., Giraud, A.L., Kleinschmidt, A., 2010. Intrinsic connectivity networks, alpha oscillations, and tonic alertness: a simultaneous electroencephalography/functional magnetic resonance imaging study. J Neurosci 30, 10243-10250.

Sadato, N., Nakamura, S., Oohashi, T., Nishina, E., Fuwamoto, Y., Waki, A., Yonekura, Y., 1998. Neural networks for generation and suppression of alpha rhythm: a PET study. Neuroreport 9, 893-897.

Sarnthein, J., Morel, A., von Stein, A., Jeanmonod, D., 2003. Thalamic theta field potentials and EEG: high thalamocortical coherence in patients with neurogenic pain, epilepsy and movement disorders. Thalamus & Related Systems 2, 231-238.

Scheeringa, R., Bastiaansen, M.C., Petersson, K.M., Oostenveld, R., Norris, D.G., Hagoort, P., 2008. Frontal theta EEG activity correlates negatively with the default mode network in resting state. Int J Psychophysiol 67, 242-251.

Schreckenberger, M., Lange-Asschenfeldt, C., Lochmann, M., Mann, K., Siessmeier, T., Buchholz, H.G., Bartenstein, P., Grunder, G., 2004. The thalamus as the generator and modulator of EEG alpha rhythm: a combined PET/EEG study with lorazepam challenge in humans. Neuroimage 22, 637-644.

Seeley, W.W., Menon, V., Schatzberg, A.F., Keller, J., Glover, G.H., Kenna, H., Reiss, A.L., Greicius, M.D., 2007. Dissociable intrinsic connectivity networks for salience processing and executive control. J Neurosci 27, 2349-2356.

Slotnick, S.D., Moo, L.R., Segal, J.B., Hart, J., Jr., 2003. Distinct prefrontal cortex activity associated with item memory and source memory for visual shapes. Brain Res Cogn Brain Res 17, 75-82.

Smith, S.M., Fox, P.T., Miller, K.L., Glahn, D.C., Fox, P.M., Mackay, C.E., Filippini, N., Watkins, K.E., Toro, R., Laird, A.R., Beckmann, C.F., 2009. Correspondence of the brain's functional architecture during activation and rest. Proc Natl Acad Sci U S A 106, 13040-13045.

Somsen, R.J., van't Klooster, B.J., van der Molen, M.W., van Leeuwen, H.M., Licht, R., 1997. Growth spurts in brain maturation during middle childhood as indexed by EEG power spectra. Biol Psychol 44, 187-209.

Steriade, M., McCormick, D.A., Sejnowski, T.J., 1993. Thalamocortical Oscillations in the Sleeping and Aroused Brain. Science 262, 679-685.

Supekar, K., Musen, M., Menon, V., 2009. Development of large-scale functional brain networks in children. PLoS Biol 7, e1000157.

Taki, Y., Hashizume, H., Sassa, Y., Takeuchi, H., Wu, K., Asano, M., Asano, K., Fukuda, H., Kawashima, R., 2011. Correlation between gray matter density-adjusted brain perfusion and age using brain MR images of 202 healthy children. Hum Brain Mapp 32, 1973-1985.

Thatcher, R.W., 1994. Cyclic cortical reorganization: Origins of human cognitive development. In: Fischer, G.D.K.W. (Ed.), Human behavior and the developing brain. Guilford Press, New York, pp. 232-266.

Thomason, M.E., Chang, C.E., Glover, G.H., Gabrieli, J.D., Greicius, M.D., Gotlib, I.H., 2008. Default-mode function and task-induced deactivation have overlapping brain substrates in children. Neuroimage 41, 1493-1503.

Tsai, Y.T., Chan, H.L., Lee, S.T., Tu, P.H., Chang, B.L., Wu, T., 2010. Significant thalamocortical coherence of sleep spindle, theta, delta, and slow oscillations in NREM sleep: recordings from the human thalamus. Neurosci Lett 485, 173-177.

Tyvaert, L., Hawco, C., Kobayashi, E., LeVan, P., Dubeau, F., Gotman, J., 2008. Different structures involved during ictal and interictal epileptic activity in malformations of cortical development: an EEG–fMRI study. Brain 131, 2042-2060.

Van Dijk, K.R., Hedden, T., Venkataraman, A., Evans, K.C., Lazar, S.W., Buckner, R.L., 2010. Intrinsic functional connectivity as a tool for human connectomics: theory, properties, and optimization. J Neurophysiol 103, 297-321.

Wackermann, J., Matousek, M., 1998. From the 'EEG age' to a rational scale of brain electric maturation. Electroencephalogr Clin Neurophysiol 107, 415-421.

Whitford, T.J., Rennie, C.J., Grieve, S.M., Clark, C.R., Gordon, E., Williams, L.M., 2007. Brain maturation in adolescence: concurrent changes in neuroanatomy and neurophysiology. Hum Brain Mapp 28, 228-237.

Yang, H., Long, X.Y., Yang, Y., Yan, H., Zhu, C.Z., Zhou, X.P., Zang, Y.F., Gong, Q.Y., 2007. Amplitude of low frequency fluctuation within visual areas revealed by resting-state functional MRI. Neuroimage 36, 144-152.

Zang, Y.F., He, Y., Zhu, C.Z., Cao, Q.J., Sui, M.Q., Liang, M., Tian, L.X., Jiang, T.Z., Wang, Y.F., 2007. Altered baseline brain activity in children with ADHD revealed by resting-state functional MRI. Brain Dev 29, 83-91.

Zuo, X.N., Di Martino, A., Kelly, C., Shehzad, Z.E., Gee, D.G., Klein, D.F., Castellanos, F.X., Biswal, B.B., Milham, M.P., 2010. The oscillating brain: complex and reliable. Neuroimage 49, 1432-1445.

Supplementary material

Supplementary Table S1. Table of anatomic labels corresponding to ANOVA results (Fig. 2.2). Anatomic label corresponds to the peak voxel of the cluster. Maximally 3 peak voxels of a cluster are listed.

Cluste size	Peak F-value	MNI-coordinate (x, y, z)	Region (Brodmann Area)
Group			
90	10.5	(15, -84, 15)	r Cuneus (18)
Condition			
96	37.25	(-27, -9, -21)	l Amygdala
2628	31.96	(27, -12, 75)	r Superior Frontal G. (6)
	28.71	(12, -24, 81)	No lable
	27.13	(24, -24, 78)	r Precentral G. (6)
193	28.6	(24, -15, -24)	r Parahippocampal G. (28)
78	24.1	(15, -69, 39)	r Precuneus (7)
203	23.59	(-15, -45, -3)	l Lingual G. (19)
42	18.97	(-36, 54, 18)	l Superior Frontal G. (10)
128	18.7	(12, -51, -3)	r Culmen
	15.13	(12, -39, -6)	r Culmen
224	17.23	(39, -21, 15)	r Insula (13)
	16.9	(63, -18, 6)	r Superior Temporal G. (22)
	16.32	(39, -6, 12)	r Insula (13)
59	16.77	(0, -21, 24)	l Cingulate G. (23)
	14.95	(3, -33, 18)	r Posterior Cingulate (23)
27	15.34	(33, 51, 33)	r Superior Frontal G. (9)
Frequency			
29118	17.05	(18, -84, 3)	r Cuneus (17)
	17.01	(-21, -30, 69)	l Precentral G. (4)
	16.44	(9, 6, 48)	r Medial Frontal G. (32)
51	7.32	(24, -9, -27)	r Parahippocampal G. (35)
37	5.31	(-33, 57, 6)	l Middle Frontal G. (10)
Group x Frequency			
29	3.92	(57, -60, 6)	r Middle Temporal G. (39)
26	3.32	(-15, -66, 3)	l Lingual G. (19)
Condition x Frequency			
2453	9.23	(9, -30, 69)	r Medial Frontal G. (6)
	8.08	(-9, -21, 75)	l Superior Frontal G. (6)
	7.64	(-3, -27, 69)	l Medial Frontal G. (6)
86	8.16	(33, 18, 6)	r Claustrum
163	8.13	(33, 45, 36)	r Superior Frontal G. (9)
	5.21	(39, 51, 24)	r Middle Frontal G. (10)
138	6.96	(15, -6, 9)	r Thalamus
	5.02	(-12, -9, 9)	l Thalamus
	4.53	(0, -18, 6)	l Thalamus
685	6.68	(9, -78, 24)	r Cuneus (18)
	6.42	(-6, -99, 3)	l Cuneus (18)
	6.32	(18, -78, 30)	r Cuneus (7)
69	6.63	(0, 60, 30)	l Superior Frontal G. (9)
94	6.44	(60, -36, 42)	r Inferior Parietal L. (40)
	5.47	(57, -39, 54)	r Postcentral G. (40)
138	6.42	(-66, -33, 6)	l Superior Temporal G. (22)
	5.9	(-54, -39, 12)	l Superior Temporal G. (22)
101	5.94	(-51, 6, 3)	l Superior Temporal G. (22)
	5.72	(-33, 15, 6)	l Claustrum

table continues on next page

table continued from the previous page

Cluste size	**Peak F-value**	**MNI-coordinate (x, y, z)**	**Region (Brodmann Area)**
77	5.86	(-33, 42, 18)	l Middle Frontal G. (10)
	5.8	(-33, 48, 36)	l Superior Frontal G. (9)
98	5.86	(6, 18, 36)	r Cingulate G. (32)
	5.71	(6, 15, 45)	r Cingulate G. (32)
45	5.8	(12, -27, 39)	r Cingulate G. (31)
113	5.65	(66, -24, -3)	r Superior Temporal G. (21)
	5.23	(48, -27, 0)	r Superior Temporal G. (22)
	5.19	(63, -12, -6)	r Superior Temporal G. (21)
294	5.56	(-6, -51, 3)	l Posterior Cingulate (29)
	5.37	(-6, -48, 24)	l Posterior Cingulate (23)
	5.18	(18, -48, -6)	r Lingual G. (19)
99	5.53	(-18, -81, 30)	l Cuneus (7)
	4.57	(-24, -84, 15)	l Cuneus (18)
	4.5	(-21, -75, 21)	l Precuneus (31)
98	5.22	(-48, -63, 33)	l Angular G. (39)
	5.1	(-48, -54, 21)	l Supramarginal G. (40)
Group x Condition x Frequency			
28	3.57	(6, 57, -9)	r Medial Frontal G. (10)
	3.35	(6, 60, 3)	r Medial Frontal G.

Supplementary Table S2. Table of anatomic labels corresponding to group differences of EEG-BOLD coupling (Fig. 2.3B). The table is ordered by group difference, condition, frequency and contrast direction. Anatomic label corresponds to the peak voxel of the cluster. Maximally 3 peak voxels of a cluster are listed.

Cluste size	Peak T-value	MNI-coordinate (x, y, z)	Region (Brodmann Area)
		Children <> Adults	
Children < Adults EO Theta			
49	3.7	(-6, -84, 21)	l Cuneus (18)
Children > Adults EO Theta			
30	3.75	(45, 30, 45)	r Middle Frontal G. (8)
Children > Adults EO Beta2			
102	4.11	(-60, -54, 33)	l Supramarginal G. (40)
Children < Adults EC Alpha2			
31	3.55	(-6, -9, 3)	l Thalamus
Children > Adults EC Alpha2			
85	3.91	(-42, -12, 36)	l Precentral G. (6)
	3.81	(-51, -12, 39)	l Precentral G. (6)
114	3.82	(54, -9, 54)	r Precentral G. (6)
	3.81	(48, -9, 45)	r Precentral G. (6)
	3.29	(63, -3, 30)	r Precentral G. (6)
170	3.65	(-15, -66, 3)	l Lingual G. (19)
	3.65	(-21, -87, -3)	l Lingual G. (17)
	3.34	(-18, -87, 9)	l Cuneus (17)
Children < Adults EC Beta1			
107	4.36	(21, 15, 63)	r Superior Frontal G. (6)
57	3.98	(-15, 12, 57)	l Superior Frontal G. (6)
	3.68	(-21, 3, 54)	l Medial Frontal G. (6)
	3.16	(-30, 9, 60)	l Middle Frontal G. (6)
118	3.84	(9, -3, 3)	r Thalamus
	3.71	(-9, -6, 0)	l Thalamus
	3.69	(-12, 0, 9)	l Caudate Body
27	3.38	(-21, 9, -12)	l Lentiform Nucleus
	3.24	(-24, 6, -3)	l Lentiform Nucleus
Children > Adults EC Beta1			
43	3.79	(-42, -12, 33)	l Precentral G. (6)
Children > Adults EC Beta2			
50	4.08	(-57, -54, 45)	l Inferior Parietal L. (40)
	3.96	(-51, -57, 51)	l Inferior Parietal L. (40)
27	3.75	(48, 36, -12)	r Inferior Frontal G. (47)
	3.42	(51, 39, 0)	r Inferior Frontal G. (46)
27	3.51	(6, 36, 39)	r Medial Frontal G. (6)
		Children <> Adolescents	
Children < Adolescents EO Alpha2			
30	3.91	(-3, -45, 15)	l Posterior Cingulate (29)
Children > Adolescents EO Beta1			

table continues on next page

table continued from the previous page

Cluste size	Peak T-value	MNI-coordinate (x, y, z)	Region (Brodmann Area)
40	3.46	(-6, -84, -9)	l Lingual G. (18)
	3.36	(-18, -90, -6)	l Lingual G. (17)
Children > Adolescents EO Beta2			
60	3.9	(12, -84, -9)	r Lingual G. (18)
107	3.67	(-18, -90, -6)	l Lingual G. (17)
	3.63	(-30, -93, 0)	l Middle Occipital G. (18)
	3.39	(-15, -99, 15)	l Cuneus (18)
Children > Adolescents EC Alpha1			
101	4.22	(-45, -42, 12)	l Superior Temporal G. (41)
	3.37	(-48, -60, 9)	l Middle Temporal G. (39)
Children > Adolescents EC Alpha2			
1652	4.84	(-27, -93, -6)	l Inferior Occipital G. (18)
	4.74	(27, -93, 0)	r Middle Occipital G. (18)
	4.29	(24, -60, -3)	r Lingual G. (19)
565	4.69	(6, -27, 60)	r Medial Frontal G. (6)
	4.17	(-12, -33, 66)	l Precentral G. (4)
	3.91	(12, -33, 75)	r Precentral G. (4)
390	4.62	(-12, -51, -6)	l Culmen
	3.68	(-15, -69, -12)	l Lingual G. (18)
230	4.29	(-66, -30, 3)	l Superior Temporal G. (22)
	4.15	(-57, -39, 9)	l Superior Temporal G. (22)
	3.58	(-60, -9, -12)	l Middle Temporal G. (21)
224	4.19	(60, -18, -9)	r Middle Temporal G. (21)
	4.17	(51, -24, -9)	r Superior Temporal G. (21)
	3.73	(63, -6, -15)	r Middle Temporal G. (21)
180	4.07	(51, -9, 39)	r Precentral G. (6)
	3.8	(63, -6, 36)	r Precentral G. (6)
	3.71	(33, -15, 45)	r Middle Frontal G. (6)
89	3.9	(-54, -12, 36)	l Precentral G. (6)
	3.35	(-39, -21, 36)	l Precentral G. (4)
31	3.5	(-45, -60, 9)	l Middle Temporal G. (39)
	3.35	(-51, -66, 15)	l Middle Temporal G. (19)
Children < Adolescents EC Beta1			
41	3.72	(0, -6, 0)	l Thalamus
	3.5	(0, -18, 3)	l Thalamus
	3.24	(-9, -12, 12)	l Thalamus
Children > Adolescents EC Beta1			
737	4.56	(15, -84, 18)	r Cuneus (18)
	4.11	(27, -60, -3)	r Lingual G. (19)
	3.71	(18, -63, -15)	r Culmen
153	3.86	(-39, -21, 36)	l Precentral G. (4)
	3.79	(-54, -6, 21)	l Precentral G. (4)
	3.27	(-48, -21, 48)	l Postcentral G. (3)
108	3.83	(63, -6, 33)	r Precentral G. (6)
	3.76	(51, -12, 36)	r Precentral G. (6)
106	3.63	(-18, -54, -9)	l Parahippocampal G. (19)
	3.62	(-18, -66, -12)	l Lingual G. (19)
59	3.61	(51, -27, -12)	r Middle Temporal G. (21)
	3.57	(60, -27, -9)	r Middle Temporal G. (21)
	3.17	(60, -15, -12)	r Middle Temporal G. (21)
36	3.55	(45, -36, 3)	r Superior Temporal G. (41)
	3.47	(48, -42, 15)	r Insula (13)

table continues on next page

table continued from the previous page

Cluste size	Peak T-value	MNI-coordinate (x, y, z)	Region (Brodmann Area)
27	3.44	(-18, -66, 9)	l Posterior Cingulate (30)
	3.15	(-12, -72, 15)	l Cuneus (18)
Children < Adolescents EC Beta2			
84	4.12	(0, -3, 3)	l Thalamus
	3.63	(6, -30, 3)	r Thalamus
	3.59	(-3, -30, 6)	l Thalamus
Children > Adolescents EC Beta2			
193	4.64	(-57, -6, 21)	l Precentral G. (4)
	3.89	(-60, -9, 33)	l Precentral G. (6)
	3.73	(-39, -18, 36)	l Precentral G. (6)
1422	4.61	(-12, -48, -6)	l Culmen
	4.6	(24, -60, -3)	r Lingual G. (19)
	4.51	(12, -84, 15)	r Cuneus (18)
47	4.55	(45, -9, 63)	r Precentral G. (6)
	3.71	(33, -15, 72)	r Precentral G. (6)
583	4.43	(66, -15, 18)	r Postcentral G. (43)
	4.42	(51, 0, 18)	r Inferior Frontal G. (44)
	3.92	(54, -12, 21)	r Postcentral G. (43)
		Adolescents <> Adults	
Adolescents < Adults EO Delta			
32	3.86	(-45, 9, 54)	l Middle Frontal G. (6)
68	3.82	(-6, 63, 15)	l Medial Frontal G. (10)
	3.8	(-6, 63, 27)	l Superior Frontal G. (10)
46	3.69	(-42, -63, 48)	l Superior Parietal L. (7)
Adolescents > Adults EO Alpha1			
50	4.12	(42, -54, 45)	r Inferior Parietal L. (40)
	3.76	(39, -63, 60)	r Superior Parietal L. (7)
Adolescents < AdultsEO Beta1			
60	4.05	(21, -81, 12)	r Cuneus (17)
147	4.01	(15, -87, -9)	r Lingual G. (18)
	3.58	(33, -87, -9)	r Inferior Occipital G. (18)
	3.55	(33, -78, -15)	r Fusiform G. (19)
265	3.95	(-24, -93, 6)	l Middle Occipital G. (18)
	3.83	(-6, -84, -9)	l Lingual G. (18)
	3.82	(-18, -99, 12)	l Middle Occipital G. (18)
67	3.88	(27, -48, 72)	r Postcentral G. (5)
	3.75	(15, -42, 78)	No lable
29	3.7	(-24, -45, 75)	l Postcentral G. (5)
	3.57	(-30, -39, 63)	l Postcentral G. (3)
Adolescents < Adults EC Alpha2			
29	3.83	(-12, -42, -6)	l Culmen
Adolescents < Adults EC Beta1			
27	3.49	(9, -42, 60)	r Paracentral L. (5)
Adolescents < Adults EC Beta2			
53	3.86	(66, -15, 12)	r Transverse Temporal G. (42)
53	3.44	(3, -93, 15)	r Cuneus (18)

table continues on next page

table continued from the previous page

Cluste size	**Peak T-value**	**MNI-coordinate (x, y, z)**	**Region (Brodmann Area)**
	3.37	(9, -87, 15)	r Cuneus (18)

Supplementary Table S3. Table of anatomic labels corresponding to maturation-independent EEG-BOLD signal correlations (Fig. 2.4A and B). Table is ordered by condition, frequency and correlation sign. Anatomic label corresponds to the peak voxel of the cluster. Maximally 3 peak voxels of a cluster are listed.

Cluste size	Peak T-value	MNI-coordinate (x, y, z)	Region (Brodmann Area)
EO Delta positive			
471	4.76	(9, 6, 48)	r Medial Frontal G. (32)
	4.71	(3, 21, 30)	r Anterior Cingulate (24)
65	4.54	(0, -63, -15)	l Culmen
	3.81	(9, -57, -18)	r Declive
44	3.9	(39, 9, 12)	r Insula (13)
	3.23	(57, 3, 6)	r Superior Temporal G. (22)
26	3.61	(-54, -6, 15)	l Precentral G. (4)
	3.25	(-57, 0, 9)	l Precentral G. (6)
25	3.47	(51, -33, 24)	r Inferior Parietal L. (40)
EO Delta negative			
129	5.83	(-48, 42, -6)	l Inferior Frontal G. (47)
563	5.11	(-45, -51, 42)	l Inferior Parietal L. (40)
	4.15	(-24, -78, 48)	l Superior Parietal L. (7)
	3.79	(-30, -84, 36)	l Precuneus (19)
788	4.98	(27, -78, 54)	r Precuneus (7)
	4.95	(45, -57, 36)	r Inferior Parietal L. (40)
	4.21	(30, -84, 45)	r Precuneus (19)
415	4.56	(24, 24, 60)	r Superior Frontal G. (6)
	4.39	(48, 33, 21)	r Middle Frontal G. (46)
	4.34	(51, 24, 33)	r Middle Frontal G. (9)
139	4.32	(39, 42, -9)	r Middle Frontal G. (47)
	4.19	(48, 48, -3)	r Inferior Frontal G. (10)
	3.91	(42, 54, 0)	r Middle Frontal G. (10)
274	4.08	(-18, 27, 57)	l Superior Frontal G. (6)
	4.08	(-51, 24, 27)	l Middle Frontal G. (46)
	4.06	(-48, 15, 48)	l Middle Frontal G. (8)
EO Theta positive			
213	6.56	(-3, -63, -15)	l Culmen
	6.45	(6, -63, -15)	r Culmen
5378	6.09	(-36, -12, 24)	l Insula (13)
	5.96	(-54, -6, 15)	l Precentral G. (4)
	5.75	(12, 9, 45)	r Cingulate G. (32)
195	4.23	(18, -27, 81)	No lable
	4.01	(27, -21, 75)	r Precentral G. (6)
	3.92	(21, -15, 78)	r Superior Frontal G. (6)
49	4.08	(-24, -9, -18)	l Amygdala
139	4.04	(39, -54, 0)	r Temporal Lobe Sub-Gyral
	3.96	(36, -63, 3)	r Occipital Lobe Sub-Gyral
	3.8	(36, -36, -3)	r Caudate Tail
EO Theat negative			
2298	7.01	(-51, -60, 36)	l Supramarginal G. (40)
	6.2	(-3, -33, 39)	l Cingulate G. (31)
	5.98	(-42, -63, 54)	l Superior Parietal L. (7)
1639	5.68	(-45, 18, 48)	l Middle Frontal G. (8)
	5.59	(-24, 24, 60)	l Superior Frontal G. (8)
	5.41	(-30, 21, 54)	l Superior Frontal G. (8)
34	3.97	(48, 39, -9)	r Middle Frontal G. (47)
EO Alpha1 positive			

table continues on next page

table continued from the previous page

Cluste size	Peak T-value	MNI-coordinate (x, y, z)	Region (Brodmann Area)
45	5.13	(-27, -9, -21)	l Amygdala
61	4.49	(24, -12, -21)	r Parahippocampal G. (28)
EO Alpha1 negative			
2198	6.59	(-12, -81, 51)	l Precuneus (7)
	6.31	(15, -75, 48)	r Precuneus (7)
	5.92	(9, -69, 63)	r Precuneus (7)
101	5.5	(-60, -42, 36)	l Inferior Parietal L. (40)
309	4.57	(-39, 24, 0)	l Inferior Frontal G. (47)
	4.23	(-39, 45, 12)	l Middle Frontal G. (10)
	3.33	(-45, 9, 9)	l Precentral G. (44)
189	4.43	(9, -33, 45)	r Paracentral L. (31)
	3.56	(6, -36, 21)	r Posterior Cingulate (23)
	3.5	(-6, -33, 42)	l Cingulate G. (31)
247	4.35	(9, -87, 6)	r Cuneus (17)
	4.17	(18, -75, -12)	r Lingual G. (18)
	3.82	(-6, -96, 0)	l Cuneus (17)
36	3.79	(-48, 30, 33)	l Middle Frontal G. (9)
	3.33	(-33, 48, 36)	l Superior Frontal G. (9)
72	3.71	(51, 42, 9)	r Inferior Frontal G. (46)
	3.65	(45, 51, -3)	r Middle Frontal G. (10)
45	3.66	(48, 15, 9)	r Precentral G. (44)
	3.25	(33, 18, 6)	r Claustrum
63	3.64	(-57, -60, 3)	l Middle Temporal G. (21)
	3.63	(-48, -69, -6)	l Inferior Temporal G. (37)
28	3.6	(-33, -51, 48)	l Superior Parietal L. (7)
EO Alpha2 negative			
3404	7.18	(12, -78, 48)	r Precuneus (7)
	6.09	(-9, -81, 51)	l Precuneus (7)
	5.98	(27, -87, 30)	r Cuneus (19)
902	6.17	(33, 48, 36)	r Superior Frontal G. (9)
	5.64	(39, 54, 24)	r Middle Frontal G. (10)
	5.14	(30, 21, 6)	r Claustrum
442	5.73	(57, -39, 42)	r Inferior Parietal L. (40)
	5.04	(51, -42, 60)	r Inferior Parietal L. (40)
413	5.36	(-33, 48, 36)	l Superior Frontal G. (9)
	5.36	(-36, 51, 21)	l Middle Frontal G. (10)
	3.68	(-51, 24, 36)	l Middle Frontal G. (9)
183	5.09	(45, 6, 51)	r Middle Frontal G. (6)
250	5.08	(12, -33, 45)	r Cingulate G. (31)
	3.72	(-6, -18, 33)	l Cingulate G. (23)
294	4.64	(-42, 12, 12)	l Insula (13)
	4.43	(-33, 18, 3)	l Claustrum
	3.79	(-30, 27, 6)	l Inferior Frontal G. (45)
75	4.31	(-63, -42, 30)	l Inferior Parietal L. (40)
	4.27	(-54, -39, 45)	l Inferior Parietal L. (40)
133	4.06	(6, 18, 51)	r Medial Frontal G. (8)
	4.04	(6, 18, 33)	r Cingulate G. (24)
EO Beat1 negative			
8742	8.46	(-21, -75, 45)	l Precuneus (7)
	7.92	(30, -72, 36)	r Precuneus (19)
	7.86	(30, -60, 51)	r Superior Parietal L. (7)
2317	7.76	(-51, 18, 36)	l Middle Frontal G. (9)
	6.1	(-45, 45, 0)	l Inferior Frontal G. (10)
	5.84	(-30, 6, 54)	l Middle Frontal G. (6)

table continues on next page

table continued from the previous page

Cluste size	Peak T-value	MNI-coordinate (x, y, z)	Region (Brodmann Area)
1858	6.3	(30, 12, 63)	r Middle Frontal G. (6)
	5.9	(51, 39, 18)	r Middle Frontal G. (46)
	5.79	(51, 21, 36)	r Middle Frontal G. (9)
25	3.95	(18, -30, 0)	r Thalamus
EO Beat2 negative			
455	5.49	(-15, -69, 39)	l Precuneus (7)
	3.6	(-30, -78, 27)	l Superior Occipital G. (39)
	3.43	(-30, -90, 21)	l Cuneus (19)
930	5.24	(15, -72, 45)	r Precuneus (7)
	4.64	(33, -84, 21)	r Middle Occipital G. (19)
	4.56	(30, -63, 36)	r Angular G. (39)
203	4.25	(6, -87, 3)	r Cuneus (17)
	3.39	(12, -102, 9)	r Cuneus (18)
323	4.21	(6, -36, 24)	r Posterior Cingulate (23)
	4.12	(-6, -27, 27)	l Cingulate G. (23)
	3.9	(9, -24, 27)	r Cingulate G. (23)
52	3.85	(-45, 33, 36)	l Middle Frontal G. (9)
	3.25	(-51, 18, 36)	l Middle Frontal G. (9)
48	3.59	(-33, -51, 45)	l Inferior Parietal L. (40)
EC Delta positive			
395	5.25	(3, 18, 33)	r Cingulate G. (32)
	4.78	(9, 6, 39)	r Cingulate G. (24)
	4.24	(-18, 12, 27)	l Caudate Body
212	4.71	(0, 0, 0)	r Anterior Cingulate (25)
	3.56	(12, -6, 9)	r Thalamus
	3.45	(-6, -9, 15)	l Thalamus
43	4.25	(-36, 9, 9)	l Insula (13)
66	3.97	(33, 12, 6)	r Claustrum
	3.3	(27, 30, 9)	r Insula (45)
35	3.83	(6, -27, -18)	r Midbrain
	3.37	(-3, -27, -21)	l Midbrain
40	3.82	(-21, 42, -6)	l Anterior Cingulate (32)
	3.27	(-24, 30, 9)	l Claustrum
EC Delta negative			
74	3.83	(42, -33, 42)	r Inferior Parietal L. (40)
	3.13	(51, -21, 45)	r Postcentral G. (3)
45	3.74	(36, -48, 66)	r Postcentral G. (5)
	3.67	(30, -54, 69)	r Superior Parietal L. (7)
81	3.68	(-30, -36, 45)	l Postcentral G. (3)
	3.47	(-39, -39, 54)	l Inferior Parietal L. (40)
	3.23	(-36, -30, 39)	l Postcentral G. (2)
56	3.67	(6, -27, 63)	r Medial Frontal G. (6)
	3.52	(9, -24, 75)	r Medial Frontal G. (6)
EC Theta positive			
3621	5.73	(-21, -27, 66)	l Precentral G. (4)
	5.72	(21, -24, 63)	r Precentral G. (4)
	5.46	(-33, -21, 72)	l Precentral G. (6)
87	4.39	(24, -99, 3)	r Middle Occipital G. (18)
	3.51	(21, -99, 18)	r Cuneus (19)
61	4.32	(-30, -72, 9)	l Posterior Cingulate (30)
77	4.29	(15, -57, -18)	r Declive
	3.77	(6, -66, -12)	r Culmen
	3.49	(-3, -66, -12)	l Culmen of Vermis

table continues on next page

table continued from the previous page

Cluste size	Peak T-value	MNI-coordinate (x, y, z)	Region (Brodmann Area)
112	4.25	(-21, 24, 18)	l Caudate Body
	3.81	(-21, 33, 6)	l Frontal Lobe Sub-Gyral
	3.79	(-24, 39, -3)	l Middle Frontal G. (11)
139	3.91	(-12, -99, 24)	l Cuneus (19)
	3.65	(-15, -99, 12)	l Middle Occipital G. (18)
39	3.78	(33, -72, 9)	r Temporal Lobe Sub-Gyral
EC Theat negative			
118	4.47	(45, 18, 42)	r Precentral G. (9)
258	4.46	(-51, -51, 45)	l Inferior Parietal L. (40)
	4.29	(-39, -60, 60)	l Superior Parietal L. (7)
	3.86	(-27, -81, 48)	l Superior Parietal L. (7)
276	4.33	(12, 30, 63)	r Superior Frontal G. (6)
	4.2	(24, 24, 57)	r Superior Frontal G. (8)
	3.91	(0, 33, 45)	l Medial Frontal G. (8)
112	4.21	(-45, 18, 45)	l Middle Frontal G. (8)
	3.81	(-27, 24, 57)	l Superior Frontal G. (8)
25	4.1	(-60, -57, -6)	l Inferior Temporal G. (37)
	3.39	(-60, -45, -9)	l Middle Temporal G. (21)
68	3.77	(54, -51, 45)	r Inferior Parietal L. (40)
	3.59	(57, -48, 36)	r Supramarginal G. (40)
28	3.48	(39, -66, 57)	r Superior Parietal L. (7)
EC Alpha1 positive			
30	3.59	(-24, -39, 21)	l Caudate Tail
EC Alpha1 negative			
932	5.34	(-3, -72, 57)	l Superior Parietal L. (7)
	5.31	(-6, -54, 72)	l Postcentral G. (7)
	4.78	(9, -75, 57)	r Superior Parietal L. (7)
103	4.83	(-42, -48, 63)	l Postcentral G. (5)
83	4.01	(42, -78, 30)	r Angular G. (39)
41	3.98	(15, -33, -6)	r Parahippocampal G. (30)
52	3.89	(57, -54, 9)	r Superior Temporal G. (22)
	3.19	(63, -57, -3)	r Middle Temporal G. (21)
38	3.73	(42, -45, 57)	r Inferior Parietal L. (40)
34	3.64	(-48, 27, 15)	l Inferior Frontal G. (46)
EC Alpha2 positive			
334	6.96	(0, -6, 3)	l Thalamus
EC Alpha2 negative			
19832	7.23	(24, -75, 27)	r Precuneus (31)
	7.22	(15, -78, 21)	r Cuneus (18)
	6.82	(21, -45, -6)	r Parahippocampal G. (19)
150	4.27	(57, 30, 12)	r Inferior Frontal G. (46)
EC Beta1 positive			
412	6.64	(0, -6, 3)	l Thalamus
	4.72	(12, -9, 12)	r Thalamus
	3.58	(-27, -12, 27)	l Extra-Nuclear
62	4.74	(-24, -45, 24)	l Cingulate G. (31)
EC Beat1 negative			
23338	8.18	(-39, -42, 60)	l Postcentral G. (2)
	7.41	(-21, -78, 48)	l Precuneus (7)
	7.19	(39, -33, 42)	r Inferior Parietal L. (40)

table continues on next page

table continued from the previous page

Cluste size	**Peak T-value**	**MNI-coordinate (x, y, z)**	**Region (Brodmann Area)**
38	3.93	(-12, 63, 9)	l Medial Frontal G. (10)
28	3.88	(-33, 0, -24)	l Amygdala
46	3.73	(12, 66, 15)	r Medial Frontal G. (10)
EC Beta2 positive			
558	6.19	(-3, -6, 0)	l Thalamus
	5.47	(-12, -12, 12)	l Thalamus
	5.45	(0, -18, 6)	l Thalamus
EC Beta2 negative			
17534	6.86	(6, -33, 63)	r Paracentral L. (6)
	6.82	(27, -12, 72)	r Superior Frontal G. (6)
	6.66	(21, -75, 27)	r Precuneus (31)
48	4.14	(27, -12, -30)	r Parahippocampal G. (35)
	4.12	(24, 0, -30)	r Amygdala
28	3.48	(-21, -30, -9)	l Parahippocampal G. (27)
	3.37	(-30, -18, -21)	l Hippocampus
	3.34	(-21, -21, -15)	l Parahippocampal G. (35)